Program

June 2 (Sun)		
Excursion		
June 3 (Mon)		
9:00 ~ 11:50	Qualifying Examination (QE) of GP-EES students (@*N204*)	
11:50 ~ 14:50	Poster Session (@*Aoba Science Hall*) & Lunch Break	
14:50 ~ 17:40	Qualifying Examination (QE) of GP-EES students (@*N204*)	
18:00 ~ 20:00	Discussion (@*AOSIS*)	
June 4 (Tue) (@*Aoba Science Hall*)		
9:00 ~ 9:10	Toshio SUGA	Opening Remarks
Session 1 (Chair: K. EMOTO)		
9:10 ~ 9:40	Benoit TAISNE	Near real time remote characterisation of explosive eruptions for mitigation of impacts and loss in SE Asia
9:40 ~ 10:10	Mayumi MUJIN	In-situ observation of nucleation and growth in magma
10:10 ~ 10:30	Coffee Break	
10:30 ~ 11:00	Gerd STEINLE-NEUMANN	*P-V-T* equation-of-state to the TPa regime for liquid Fe from *ab-initio* simulations
11:00 ~ 11:30	Julien GASC	Lab-quakes during high pressure deformation experiments as analogues for intermediate and deep-focus earthquakes
11:30 ~ 13:00	Group Photo & Poster Session (@*Aoba Science Hall, N204*) & Lunch Break	
Session 2 (Chair: S. SUGIMOTO)		
13:00 ~ 13:30	Kelvin RICHARDS	Marine viruses and their impact in a turbulent ocean
13:30 ~ 14:00	Yoichi INAI	Balloon-borne observations and trajectory analysis in the lower stratosphere
14:00 ~ 14:30	Frederick BINGHAM	Interannual variability of the surface salinity maximum regions of the South Pacific and South Indian Oceans
14:30 ~ 14:50	Coffee Break	
14:50 ~ 15:20	Hideko TAKAYANAGI	New insights into Quaternary paleoceanography in the eastern Indian Ocean
Session 3 (Chair: R. TAKAGI)		
15:20 ~ 15:50	James D. P. MOORE	Hydration state of the Martian lithosphere constrained from gravity and topography
15:50 ~ 16:20	Jun MUTO	Deep afterslip and nonlinear transient mantle flow after the 2011 Tohoku-Oki Earthquake
16:20 ~ 16:40	Coffee Break	
16:40 ~ 17:10	Martha SAVAGE	Seismic anisotropy measured before and after the 2016 Kumamoto and Kaikoura earthquakes
17:10 ~ 17:40	Ross S. STEIN	Temblor: A mobile app to help the public understand and reduce their earthquake risk
17:40 ~ 17:50	Michihiko NAKAMURA	Closing Remarks

Access

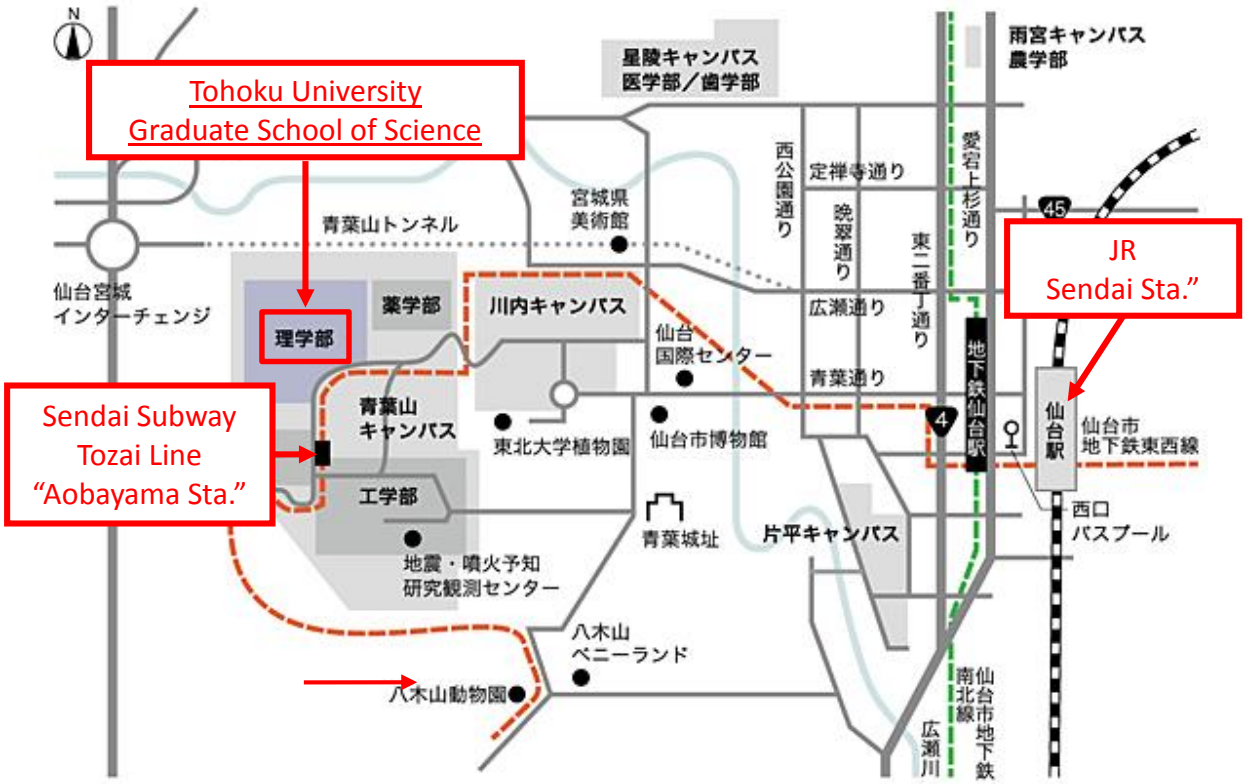

Campus map

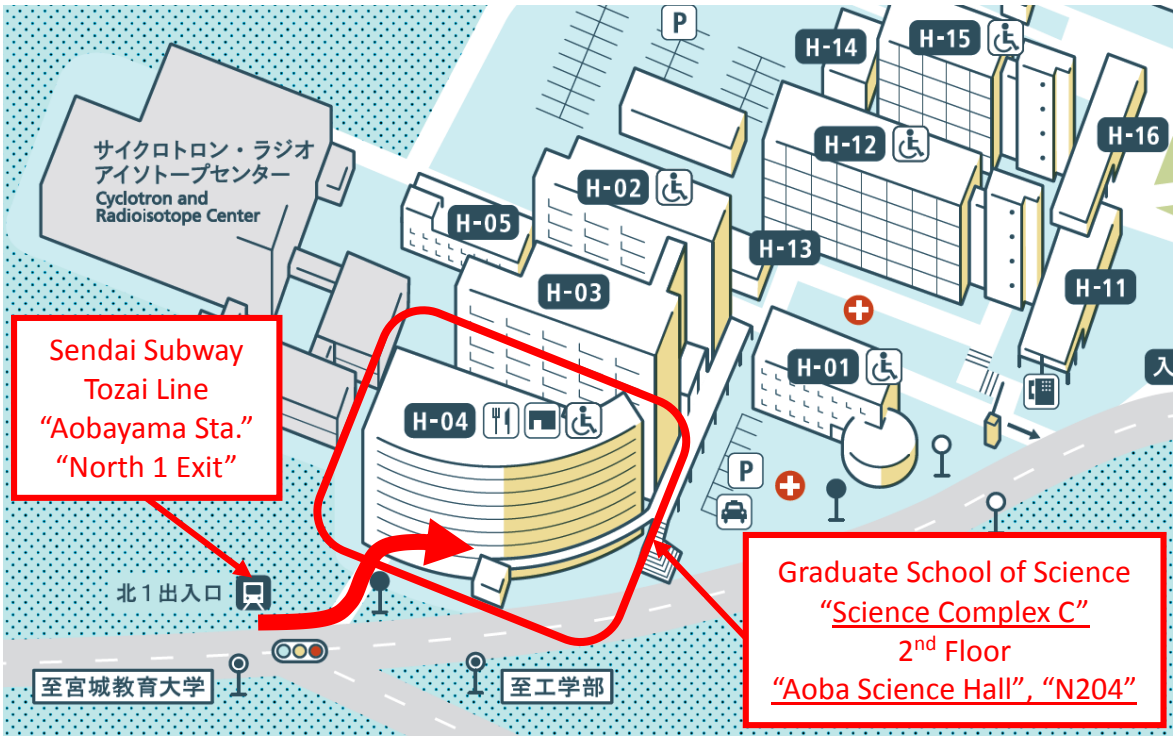

Oral presentations

Near real time remote characterisation of explosive eruptions for mitigation of impacts and loss in SE Asia

BENOIT TAISNE[1,2]

[1] Earth Observatory of Singapore
[2] Asian School of the Environment, Nanyang Technological University

I will present a new research project that aims to develop, expand upon and combine existing technologies to improve the detection, characterisation and understanding of potential impacts from explosive volcanic activity in Southeast Asia, and present information in a timely manner for efficient decision-making. It will focus on rapidly quantifying volcanic ash emissions, by harnessing a multi-technology and multi-disciplinary approach, with the aim to mitigate their short, mid and long term impacts. This project focuses on Southeast Asia where remote ground based or space based monitoring could be challenging [1]. For the short term, the project will concentrate on reducing the delay between eruption occurrence and communication of the hazard to the aviation industry. In the mid and long term, the project aims to provide information that can be used for cost-effective and predictive maintenance of jet engines as well as estimating the impact of explosive events on the ground.

Singapore, like many other smart-cities around the globe, is not immune from volcanic threats. While there are no volcanoes located within Singapore, Southeast Asia is one of the most volcanically active regions in the world and is home to 70% of the global volcanic threat. In a recent studies we identify 991 volcanoes with the potential to impact the Association of Southeast Asian Nations (ASEAN) airspace, with a 100% probability of an eruption powerful enough to produce an ash plume to 25 km or higher within any given 10 year period [2]. In 1982, a British Airways jet with 240 persons on board encountered an ash cloud at ~11 km height in west Java, Indonesia, that stalled all four of its engines and abraded its windshield and wing surfaces. The aircraft lost 7.5 km of altitude before the engines could be restarted (Global Volcanism Program, 1982). Given the very high temperatures of today's jet engines, it is not clear that an aircraft flying through the same concentration of ash today would have the same fortunate ending. Singapore is susceptible to long-range hazards from volcanic activity via volcanic ash both on the ground (with impacts for critical infrastructure, e.g., power plants and airports) and in the air (e.g., health, aviation industry). After the 1991 eruption of Pinatubo volcano in the Philippines, ash was transported to Singapore and deposited at a thickness that would, with today's criteria, close all airports and likely a large portion of the Flight Information Region (FIR). Any closure of, for example, Changi airport, and the FIR would have significant impacts on Singapore and the region as a whole, as Changi is a major aviation hub for the region.

By refining nowcasting and forecasting of volcanic ash dispersal, timely action could be taken to close or open airspace and estimate potential long term damage to aircraft and engines (reducing economical loss by taking informed decisions), give enough lead time to shut down critical infrastructure such as power plants (reducing economical loss by preventing damage to the system) as well as rapidly estimating the potential hazard and impacts of ash on the ground (informing post-disaster needs assessments and mitigating impacts for populations and infrastructure).

References

[1] Taisne B., Perttu A., Tailpied D., Caudron C., Simonini L. (2019) Atmospheric Controls on Ground- and Space-Based Remote Detection of Volcanic Ash Injection into the Atmosphere, and Link to Early Warning Systems for Aviation Hazard Mitigation. In: Le Pichon A., Blanc E., Hauchecorne A. (eds) Infrasound Monitoring for Atmospheric Studies. Springer, Cham doi:10.1007/978-3-319-75140-5_34

[2] Whelley, P., Newhall, C. G., and Bradley, K. (2015), The frequency of explosive volcanic eruptions in Southeast Asia, Bulletin of Volcanology, 77 (1). doi:10.1007/s00445-014-0893-8

In-situ observation of nucleation and growth in magma

MAYUMI MUJIN[1], MICHIHIKO NAKAMURA[1], MEGUMI MATSUMOTO[1]

[1] Department of Earth Science, Graduate School of Science, Tohoku University

Crystal nucleation and growth in magmas are fundamental but still poorly understood processes. Petrographic and experimental studies of microlites in volcanic rocks have been used to elucidate some important aspects of eruption dynamics, but few studies have addressed nucleation and growth from nanoscales. Recently, we have reported nanoscale crystals in the interstices of microlites in volcanic pyroclasts and defined those 30 nm–1 μm in width and < 30 nm in diameter as "nanolite" and "ultrananolite", respectively [1]. Because of their high crystallinity, crystallization of the nanocrystals could result in differentiation of the residual melt and increase in its viscosity at the time of magma fragmentation, thus control the volcanic eruption styles [2]. In order to understand the kinetics of nucleation and growth of nanocrystals, we have carried out in-situ observation experiments using a field emission-scanning electron microscope (FE-SEM) equipped with a high-temperature heating stag. In this presentation, we introduce some nucleation and growth processes we have succeeded in observing in-situ.

As a starting material, we used crystal-free natural volcanic glass in an andesitic pumice clast from the 1914 ("Taisho") Plinian eruption of the Sakurajima volcano, Kyusyu, Japan. The glass chemical composition in wt% is SiO_2 69.8, TiO_2 0.81, Al_2O_3 14.3, Fe_2O_3 4.28, MgO 0.89, CaO 3.11, Na_2O 4.20, and K_2O 2.61, with ~0.5 wt% dissolved H_2O [3]. We crushed the pumice clast with an agate mortar and hand-picked ~20×20 μm groundmass glass fragments. The in-situ heating experiments were performed in a JEOL JSM7100F at an acceleration voltage of 15 kV with a Protochips Aduro heating stage. The sample chamber of FE-SEM was evacuated to 9.6×10^{-5} and 60 Pa for high- (HV) and low-vacuum (LV) experiments, respectively. N_2 gas and dried air were used for vacuuming adjustment in LV runs. The temperature increased from room temperature to 850–1050 °C at 10 °C/sec and then was kept constant for approximately 1–2 hours. During the heating, secondary electron (SE) images and back-scattered electron (BSE) images were recorded through a screen record software (Blueberry Software: BB FlashBack).

In the HV runs, we found coalescence of Fe metal particles via "oriented attachment", which is one of the "non-classical" nucleation pathways observed in some aqueous solution systems in recent years (e.g., protein [4]; $CaCO_3$ [5]; Pt [6]; Pt_3Fe [7]; oxyhydroxide [8]; gypsum [9]; magnetite [10]; zeolite [11], MoS_2 [12]). This is the first observation in the silicate melt system. Crystallization via particle attachment is called "non-classical pathway" in contrast to the "classical pathway", in which addition of only monomeric chemical species is considered [13].

Under the LV runs, in which degassing is expected to be suppressed and thus melt conditions should be closer to those in natural settings, nucleation density and following growth manner of nanocrystals were principally divided into two modes. In the relatively lower temperature and dried air experiments (850 and 900 °C), Fe-oxide ultrananolites formed with a very high number density several minutes after the temperature achieved the highest experimental temperatures. The growth of the ultrananolites is limited (up to no larger than 100 nm in 1 hour). The particle attachment was not observed. At 950 and 1000 °C, in contrast, only small number of euhedral Fe-oxide and plagioclase crystals (a few to tens in each run product) were formed most possibly via heterogeneous nucleation at the sample surface, followed by rapid crystal growth. Eutectic growth of plagioclase and silica mineral was sometimes observed. These results indicate 1) that nucleation and growth of ultrananolite and nanolites are discontinuous processes, and 2) that extensive ultrananolite crystallization in andesitic magmas may proceed within several minutes under large undercooling that may be achieved in the shallow part of volcanic conduit due to extensive degassing and possibly to cooling.

References

[1] Mujin et al. (2017) Am. Min. 102, 2367–2380
[2] Di Genova et al. (2017) Nature, 552, 235–238
[3] Otsuki et al. (2015) JGR, 120(11), 7405–7424
[4] Yau and Vekilov (2001) J. Am. Chem. Soc., 123, 1280–1289, Yamazaki et al. (2017) PNAS, 114, 2154–2159
[5] Pouget et al. (2009) Science, 323, 1455–1458
[6] Zheng et al. (2009) Science, 324, 1309–1312
[7] Liao et al. (2012) Science, 336, 1011–1014
[8] Li et al. (2012) Science, 336, 1014–1018
[9] Van Driessche et al. (2012) Science, 336, 69–72
[10] Baumagartner et al. (2013) Nature materials, 12, 310–314
[11] Lupulescu and Rimer (2014) Science, 334, 729–732
[12] Fei et al. (2016) Nature communications, 7, 12206
[13] De Yoreo et al. (2015) Science, 349

Earth, Sea, and Sky V:
International Joint Graduate Program Workshop in Earth and Environmental Sciences
co-hosted by The International Joint Graduate Program in Earth and Environmental Sciences, Tohoku University (GP-EES)
and JSPS-DFG Japanese-German Graduate Externship for Research on Deep Earth Volatile Cycle
June 2-4, 2019. Aobayama Campus, Tohoku University

P-V-T equation-of-state to the TPa regime for liquid Fe from *ab-initio* simulations

GERD STEINLE-NEUMANN[1], FABIAN WAGLE[1]

[1] Bayerisches Geoinstitut, Universität Bayreuth, 95440 Bayreuth, Germany

The pressure-volume-temperature (*P-V-T*) equation-of-state (EoS) of liquid iron provides important information (reference adiabat, density ρ and higher order thermodynamic parameters) in modelling the internal structure of planetary bodies with Fe-based cores. Relevant *P*-conditions range from a few GPa (Moon, Mercury) through the 100 GPa range (Earth) to several TPa (super-Earths). Experimental data on ρ in the liquid stability field are scarce and a thermodynamic assessment of ρ depends on matching Gibbs energy along the melting line which remains controversial to this day. The alternative determination of a *P-V-T* EoS based on *ab-initio* simulations, on the other hand, suffer from the fact that ρ at ambient *P* is predicted too large by as much as 20% [e.g., 1]. Here [2], we have fitted *P-V-T-E* quadruplets from *ab-initio* molecular dynamics simulations with a self-consistent thermodynamic EoS formulation [3] and combined it with a correction formalism that accounts for the ρ-mismatch at ambient *P* [4]. As the correction is additive to the Helmholtz potential and shows the correct limiting behavior at high and low ρ, thermodynamic self-consistency of the results is not affected. Using this combination, our EoS reproduces ρ from shock-wave experiments as well as previous models, but shows a significantly improved agreement at ambient *P*, the critical point and the sole ρ measurement in the large-volume press at 4.3 GPa [5]. We explore the performance of our thermodynamic potential and various previously published EoS models for liquid iron [1,6,7] over a wide range of conditions: (i) at ambient pressure as a function of temperature, (ii) along the melting curve of Fe to 40 GPa, relevant for the cores of smaller terrestrial bodies in our solar system, (iii) along isentropes in the Earth's outer core and (iv) for the core of super-Earth Kepler-36b along a previously modelled *T*-profile in the core [8].

The correction term significantly improves the agreement of computed properties with experiments and other thermodynamic models that are based on an assessment of the phase diagram at ambient and moderate *P* [6,7], showing how *ab-initio* molecular dynamics simulations can be used at par with other techniques. For the Earth's core (Fig. 1), ρ-profiles from the various models are similar, but higher-order derivatives (acoustic velocity and Grüneisen parameter) show significant differences. For the core model of Kepler-36b, differences in ρ from various models [1,2,6,7] are negligible, for core mass they do not exceed 2%, showing robust extrapolation of all EoS models. The robustness of the different formulations of Fe equations of state at conditions of the cores of super-Earths is encouraging in the sense that it will allow for a meaningful inversion of planetary structure (e.g., core radius ratio) once relevant astronomical observations become available [9].

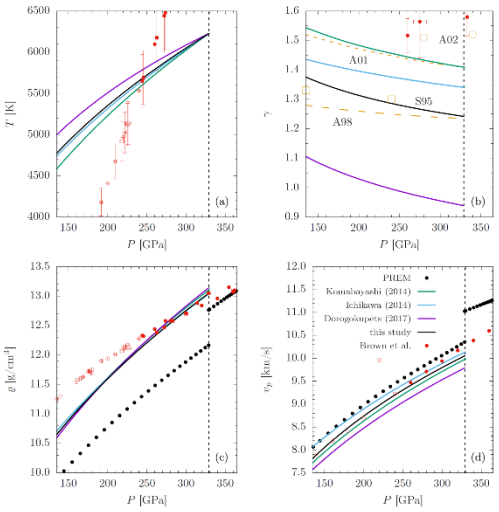

Figure 1: Temperature (a), Grüneisen parameter (b), density (c) and longitudinal wave velocity (d) for conditions of Earth‘s core, with the isentrope fixed at the melting point of Fe at *P* of the Earth‘s inner core boundary (330 GPa, 6,230 K, dashed vertical line). Black dots correspond to PREM values. Different thermodynamic models [1,2,6,7] are evaluated and compared to shock experiments [10,11], with closed symbols indicating the liquid portion of the Hugoniot. Previous estimates for the Grüneisen parameter γ by Alfè et al (2001, 2002) (A01, A02) [12,13], Stacey (1995) (S95) [14], and Anderson (1998) (A98) [15] are included in panel (b).

References [1] Ichikawa et al., JGR 119, 240 (2014); [2] Wagle & Steinle-Neumann, JGR (in press); [3] Vlček et al., PRB 85, 184201 (2012); [4] French & Mattsson, JAP 116, 013510 (2014); [5] Tateyama et al., PCM 38, 801 (2011); [6] Dorogokupets et al., Sci. Rep. 7, 41863 (2017); [7] Komabayashi, JGR 119, 4164 (2014); [8] Hakim et al., Icarus 313, 61 (2018); [9] Padovan et al., A&A 620, A178 (2018); [10] Brown & McQueen, JGR 91, 7485 (1986); [11] Brown et al., JAP 88, 5496 (2000); [12] Alfè et al., PRB 64, 045123 (2001); [13] Alfè et al., PRB 65, 165118 (2002); [14] Stacey, PEPI 89, 219 (1995); [15] Anderson, PEPI 109, 179 (1998).

Earth, Sea, and Sky V:
International Joint Graduate Program Workshop in Earth and Environmental Sciences
co-hosted by The International Joint Graduate Program in Earth and Environmental Sciences, Tohoku University (GP-EES)
and JSPS-DFG Japanese-German Graduate Externship for Research on Deep Earth Volatile Cycle
June 2-4, 2019. Aobayama Campus, Tohoku University

Lab-quakes during high pressure deformation experiments as analogues for intermediate and deep-focus earthquakes

JULIEN GASC[1], JULIEN FAUCONNIER[1], NADÈGE HILAIRET[2], THOMAS FERRAND[1], YANBIN WANG[3], CLÉMENCE DAIGRE[1], AREFEH MOAREFVAND[1], ALEXANDRE SCHUBNEL[1]

[1] Laboratoire de Géologie, ENS-CNRS, Paris, France
[2] UMET, University of Lille-CNRS, Lille, France
[3] GSE-CARS, University of Chicago, Argonne, Illinois, USA

The origin of intermediate- and deep-focus earthquakes, which occur at depths of 60-700 km along subducting slabs, remains somehow enigmatic. In the pressure and temperature conditions involved, rocks should indeed deform in a ductile fashion. For instance, dehydration embrittlement due to serpentine breakdown, was long considered a good candidate to explain intermediate-depth seismicity. However, unlike in the classic dehydration embrittlement theory, dehydration induced volume changes are negative at such depths and cannot trigger instabilities via pore pressure buildup [1,2].

In order to assess the seismic potential of serpentinites, micro-seismicity was monitored during high pressure experiments by recording Acoustic Emissions (AE's) during the deformation of natural antigorite-rich samples at pressures of 1-5 GPa. The samples show a brittle temperature window around 500°C, which seems to correlate with the very onset of the mineral's breakdown, and is therefore not associated to significant release of water. AE's are consistently collected upon faulting and extremely sharp strain localization is observed [2]. In addition, brittle faulting of partly hydrated samples can also occur with minor amounts of antigorite, due to stress percolation upon antigorite breakdown [3]. However, analysis of the acoustic signal shows that it is relatively weaker than its real-earth counterpart, once scaled relative to standard brittle faulting. Although both mechanisms can be a source of seismicity in subducting slabs, large intermediate-depth earthquakes may therefore reflect fault propagation in the adjacent peridotitic mantle.

These brittle mechanisms share major similarities with the concept of transformational faulting [4], often invoked for deep-focus earthquakes. Deep-focus lab-quake analogues were also recently characterized in a new-generation Griggs apparatus using synthetic Mg_2GeO_4 (Ge-olivine) sintered samples. Similar to the serpentinite samples, they present a brittle temperature window, where transformational faulting occurs. This window shifts to lower temperatures with decreasing strain rates, due to the effect of temperature on the olivine-spinel reaction kinetic. These results are of great interest since they help understand how metastable olivine may fault in the Earth despite much lower stresses and strain rates.

References

[1] Chernak, L.J., Hirth, G., 2011. Syndeformational antigorite dehydration produces stable fault slip. Geology 39.
[2] Gasc, J., Hilairet, N., Yu, T., Ferrand, T., Schubnel, A., Wang, Y., 2017. Faulting of natural serpentinite: Implications for intermediate-depth seismicity. Earth and Planetary Science Letters 474, 138-147.
[3] Ferrand, T.P., Hilairet, N., Incel, S., Deldicque, D., Labrousse, L., Gasc, J., Renner, J., Wang, Y., Green, H.W., II, Schubnel, A., 2017. Dehydration-driven stress transfer triggers intermediate-depth earthquakes. Nature Communications 8.
[4] Burnley, P.C., Green, H.W., Prior, D.J., 1991. Faulting associated with the olivine to spinel transformation in mg2geo4 and its implications for deep-focus earthquakes. Journal of Geophysical Research-Solid Earth and Planets 96, 425-443.

Marine viruses and their impact in a turbulent ocean

KELVIN RICHARDS[1,2]

[1] Department of Earth Science, Graduate School of Science, Tohoku University
[2] International Pacific Research Center, University of Hawai`i at Mānoa

Viruses attack marine organisms from bacteria to whales. In particular phytoplankton blooms can crash because of viral infection. Here we will explore the interaction between viruses, phytoplankton and zooplankton under bloom conditions using relatively simple models. One aspect under consideration is how viruses and zooplankton can co-exist. We should not forget that interactions take place in a fluid environment. Stirring and mixing is found to have a profound effect on viral epidemics and control the fraction of a bloom that is affected.

Balloon-borne observations and trajectory analysis in the lower stratosphere

YOICHI INAI[1]

[1] Center for Atmospheric and Oceanic Studies, Graduate School of Science, Tohoku University

The stratospheric meridional circulation, called the Brewer-Dobson circulation (BDC), which consists upwelling over the tropical region and downwelling over the polar regions, largely controls material exchange between the troposphere and stratosphere. The polluted tropospheric air masses are transported into the stratosphere through the BDC. The BDC strength and its variation are often quantified using the mean age of air (AoA), the average transit time of an air parcel since entering the stratosphere. The AoA is typically estimated from the relative concentration of a "clock tracer" (such as sulphur hexafluoride; SF_6) at any point in the stratosphere compared with that in the troposphere. Our research group have conducted balloon-borne observations to obtain chemical species, including clock tracer, distributions in the polar, midlatitude, and tropical stratosphere. Based on such observations, the long-term trend of AoA is estimated. Many numerical models have predicted that increasing concentrations of greenhouse gases are intensifying the BDC, and that AoA should therefore decrease over time, however, observational AoA estimates show no such negative trend in the Northern Hemisphere. Addressing this discrepancy, Inai (2018) [1] focuses on the mixing fraction of air masses which originating in the troposphere and stratosphere (referred to as "origin fractions") in the upper tropical tropopause layer (TTL). The origin fractions during 1980–2016 is evaluated using trajectory analysis, and the stratospheric origin fraction shows long-term variation with a positive trend between 1980 and 1999. The long-term variation in the upper TTL overall accounts for more than 20% of the discrepancy between trends in trajectory-based AoA and those in the observed AoA.

References

[1] Inai, Y.: Long-term variation in the mixing fraction of tropospheric and stratospheric air masses in the upper tropical tropopause layer, Journal of Geophysical Research: Atmospheres, 123, 4890–4909, doi:10.1029/2018JD028300, 2018.

Interannual variability of the surface salinity maximum regions of the South Pacific and South Indian Oceans

FREDERICK BINGHAM[1]

[1] Center for Marine Science, University of North Carolina Wilmington, Wilmington, NC, USA

The interannual variability of the South Indian and South Pacific Ocean sea surface salinity maximum (SSS-max) regions is studied using a combination of satellite and in situ data. Properties of the features examined include the size, strength and location, the forcing via wind stress and surface freshwater flux, subduction, and changes in the underlying subtropical circulation.

Results indicate that the South Indian SSS-max has been getting larger (by a factor of 2), saltier and has been moving poleward (by about 1.5°) and eastward (by about 5°) since the start of satellite observations of SSS. Surface currents, including Ekman transport driven by wind stress, are very weak suggesting that changes observed in the SISSS-max are a not result of changing winds or surface circulation. Changing surface freshwater flux is the more likely explanation.

During the same period the South Pacific SSS-max exhibited similar variability. It also nearly doubled in area, increased in salinity by ~0.1 pss, and moved northward by 1-2° of latitude and eastward by 10° of longitude. The change was not associated with change in air-sea freshwater flux, but rather due to changes in the advection of the subtropical gyre and South Equatorial Current (SEC), and variation in Ekman transport and Ekman pumping. There was a substantial decrease in the dynamic height difference associated with the SEC, the Ekman transport and Ekman pumping northeast of the SSS-max. The observed changes in the SSS-max appear to be linked to those of subducted subtropical underwater observed in the interior.

Thus, the two ocean regions showed similar types of changes in their position and properties. However, it appears that the changes are associated with different forcing mechanisms, Ekman transport and interior flow for the South Pacific and surface freshwater forcing for the South Indian.

New insights into Quaternary paleoceanography in the eastern Indian Ocean

HIDEKO TAKAYANAGI[1], SHIGEYUKI WAKAKI[2], TSUYOSHI ISHIKAWA[2], YASUFUMI IRYU[1]

[1] Department of Earth Science, Graduate School of Science, Tohoku University
[2] Kochi Institute for Core Sample Research, Japan Agency of Marine-Earth Science and Technology (JAMSTEC)

Surface currents, especially western boundary currents, play a significant role in the meridional transport of heat and regulate sea surface temperature (SST) variability on the ocean. Some of the well-known climate changes during the geologic past (e.g., Northern Hemisphere glaciation with subsequent global cooling) are considered to be induced by the reorganization of surface water circulation due to the opening/closure of ocean gateways. Surface currents and their related surface water masses are thus a key component of the Earth's ocean-climate system. However, their roles under millennial- to orbital-scale climate variability remain unclear. To assess behavior of surface ocean currents and their related water masses under glacial-interglacial conditions, an integrated approach on paleontological (assemblages) and geochemical (carbon, oxygen, and neodymium isotopes) records of foraminifers from shallow-water carbonates is the best way to reconstruct the strength and volume of surface currents and their related changes in surface water-mass structure.

Here, we show reconstruction of the detailed history of the Leeuwin Current (LC) and associated surface water masses off Western Australia during the Quaternary. The LC, a shallow (< 300 m depth) and narrow (< 100 km width) eastern boundary warm current, transports relatively warm, less saline, and oligotrophic tropical seawater poleward along the coastline of Western Australia. Therefore, it is crucial to understand the timing of initiation and development of the LC and to reveal their relationships to regional and global climates. We investigated carbon, oxygen, and neodymium isotopes in foraminifers from shallow-water carbonates collected off Western Australia during the International Ocean Discovery Program (IODP) Expedition 356. Taking into account of benthic foraminifer assemblages (Haller et al., 2018 [1]), we interpreted out geochemical data. Our data indicate that the LC system was initiated and established at ~1 Ma and reached to the present paleoceanographic state after the Mid-Brunhes Event (MBE) at ~0.430 Ma. Since the MBE is characterized by a further increase of ice-volume variations with large-amplitude ~100-kyr glacial-interglacial climate cycles, the LC and related surface water masses off western Australia are assumed to be related to glacioeustatic sea-level changes and northward/southward migrations of the southern subtropical front. However, our results do not show that the LC was markedly reduced in their volume or shutdown during glacial periods.

References

[1] Haller, C., Pamela, H., Hinea, A. C., Smith, C. G. (2018) Benthic foraminifera from the Carnarvon Ramp reveal variability in Leeuwin Current activity (Western Australia) since the Pliocene. Marine Micropaleontology **142**, 25–39.

Hydration state of the Martian lithosphere constrained from gravity and topography

JAMES D. P. MOORE[1], JON WADE[2], RICHARD M. PALIN[3], BRENDAN DYCK[4], ANTHONY B. WATTS[2], LARS HANSEN[2], ANDREW J. SMYE[5], JUN MUTO[6], ADAM SWITZER[1].

[1] Nanyang Technological University, Singapore, [2] University of Oxford, United Kingdom, [3] Colorado:SoM, United States, [4] SFU, Canada, [5] Penn State, United States, [6] Tohoku University, Japan

Widespread aqueous alteration of the Martian crust suggests that metamorphic hydration reactions may have played a critical role in the sequestration of water early during the planet's history. The bending strength of the Martian crust will also be affected by the presence of hydrous mineral phases, and we show that observations of the Martian gravity anomaly may be used to constrain the fate of Martian surface water.

Petrological modelling of primitive Martian basalts reveals they may hold about 25 per cent more structurally bound water than those in metamorphosed terrestrial basalts, and retain it to greater depths during burial within Mars. In excess of 9 per cent by volume of the Martian mantle may contain hydrous mineral species as a consequence of surface reactions, compared to about 4 per cent by volume of Earth's mantle. By employing flow laws associated with the predicted metamorphic mineral assemblages, we construct yield strength envelopes for these end-member crustal sections and derive the predicted elastic thicknesses, Te, a proxy for the long-term lithospheric strength of Mars. We also use spherical harmonic coefficients that describe the Martian gravity anomaly and topography fields to quantify the role of isostasy in contributing to crustal and upper mantle structure. Power spectra of these fields reveal that the gravity effect of topography and its flexural compensation contributes significantly to the observed free-air gravity anomaly spectra for spherical harmonic degree $8 < n < 50$, corresponding to wavelength $300 < \lambda < 3000$ km. The best-fit global average is for an elastic plate (flexure) model with Te of 126 ± 14 km. All isostatic models under-predict the spectra at $2 < n < 5$, and we interpret the low-order Martian gravity field, at least in part, to be the result of processes that formed the Northern Basin. By comparing the observed Martian Te to that predicted for our metamorphic mineral assemblages, we iterate on the water content until convergence. In short, we show the bending strength of Mars places constraints on the amount of hydration of the Martian crust, which in turn we use to calculate the planetary water budget.

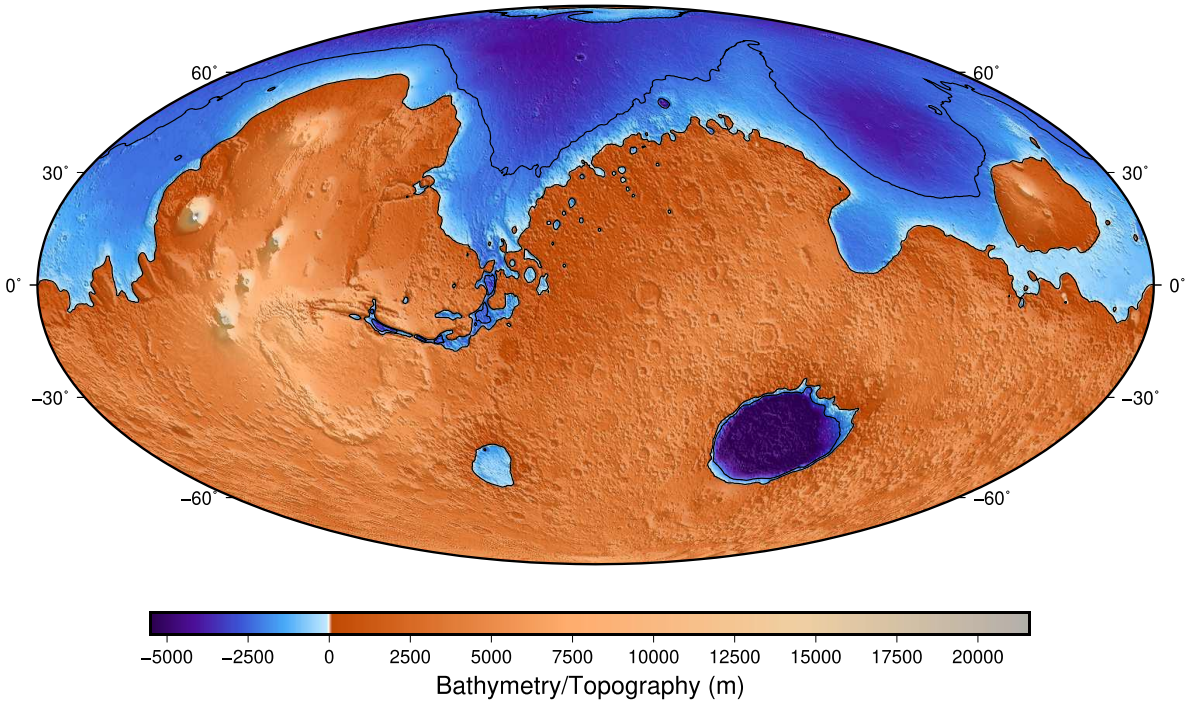

Figure 1: Topographic map of Mars, bathymetry shaded beneath putative paleoshorelines, and lower contour fill based on global equivalent sea level sequestered in hydrous mineral phases.

Deep afterslip and nonlinear transient mantle flow after the 2011 Tohoku-Oki Earthquake

JUN MUTO[1], JAMES D. P. MOORE[2], SYLVAIN BARBOT[3], TAKESHI IINUMA[4], YUSAKU OHTA[1], SYUNSUKE HORIUCHI[5], HIKARU IWAMORI[5,6,7]

[1] Tohoku University, Sendai, Japan
[2] Nanyang Technological University, Singapore
[3] University of Southern California, USA
[4] Japan Agency for Marine-Earth Science and Technology, Yokohama, Japan
[5] Japan Agency for Marine-Earth Science and Technology, Yokosuka, Japan
[6] The University of Tokyo, Tokyo, Japan
[7] Tokyo Institute of Technology, Tokyo, Japan

The largest earthquakes occur on subduction zones, and subsequent tsunamis are one of the greatest potential hazards faced by nearby coastal communities. Such great (Mw>8) and giant (Mw>9) earthquakes cause subsequent post-seismic deformation in the wide area depending on viscous structures of crustal and mantle rocks and the frictional properties of the plate interface. In particular, the progress of afterslip occurring at the down-dip of the main rupture region where coseismic stress changes are large significantly affects the post-seismic uplift of the cosesimically subsided coastal regions. However, for giant megathrust events, viscoelastic flow and deep afterslip are mechanically coupled to each other, relaxing stress changes induced by both coseismic and post-seismic slip. In the presentation, we show the role of afterslip and viscoelastic relaxation, and their interaction in the aftermath of the 2011 Mw 9.0 Tohoku earthquake. We conduct a two-dimensional analysis of the post-seismic deformation with coeval slip on the subduction interface governed by rate-strengthening friction and distributed deformation away from the fault governed by power-law rheology with transient creep. The power-law rheology with stress-driven afterslip well explains the observed post-seismic deformation field and its time series in the period 2011 to 2016. Moreover, the geodetic data indicate a persistent deep afterslip directly down-dip of the main rupture region that greatly affects the ongoing post-seismic coastal uplift. Mechanical coupling between viscoelastic relaxation and afterslip notably modifies both the afterslip distribution and the surface deformation. Thus, we find that it is important to consider the interaction of these two deformation mechanisms to more fully understand the geodynamics of the Japan trench during the early stage of the seismic cycle. Finally, we also point out that such mechanical coupling is critical to estimate the future recovery of the coseismically subsided coastal area.

Seismic Anisotropy measured before and after the 2016 Kumamoto and Kaikoura earthquakes

MARTHA SAVAGE[1], KENNY GRAHAM[1], YOSUKE AOKI[2], RICHARD ARNOLD[1], TOMOMI OKADA[3], CAROLYN BOULTON[1], MEGAN KORTINK[1], Y. IIO[4], S. MATSUMOTO[5]

[1] Victoria University of Wellington, New Zealand
[2] Earthquake Research Institute, University of Tokyo
[3] Tohoku University, Sendai 980-8578, Japan
[4] Kyoto University, Uji 611-0011, Japan
[5] Kyushu University, 2-5643-29 Shin'yama, Shimabara, Nagasaki, 855-0843, Japan

Seismic anisotropy in the crust may be caused by stress that aligns microcracks, strain that aligns minerals or structural effects. Recently both anisotropic and isotropic velocity changes have been determined after large earthquakes, and are often considered to be related to cracks that heal with time. In 2016, large earthquakes in Japan (April, Kumamoto, Kyushu) and in New Zealand (November, Kaikoura) caused widespread disruption, and also produced data with which to test some of these theories. Here we use shear wave splitting to study the seismic anisotropy before and after the 2016 Kumamoto and the Kaikoura earthquakes to study the phenomena.

In Kyushu, measurements from NIED stations between 2004-2012 yielded fast anisotropic directions that align well on average with the maximum horizontal stress from focal mechanism inversions and the maximum horizontal strain rate as measured by the GNSS system. We measured shear wave splitting on these same stations during 2016 to determine whether shear wave splitting changed over time after the Kumamoto earthquake. A few stations yielded different fast directions or increases in delay times. We are checking whether those changes are due to structural changes or can be explained by changing earthquake locations.

In New Zealand, we have measured shear wave splitting and Vp/Vs ratios on permanent stations near the Kaikoura earthquake rupture region between 2013 and 2018. Some stations exhibit apparent changes in fast direction, but spatial averaging does not yield strong changes in fast directions with time. Delay times and Vp/Vs ratios both increased after the M=6.5 and M=6.6 Cook Strait earthquakes and after the M=7.8 Kaikoura earthquake. After the Cook Strait earthquakes, measurements returned to background levels within several months. But by the end of 2017 the measurements had not yet returned to normal. Laboratory measurements suggest that crack healing should yield more rapid recovery, and we are exploring whether aftershocks help to keep the cracks open.

Temblor: A mobile app to help the public understand and reduce their earthquake risk

ROSS S. STEIN[1,2] VOLKAN SEVILGEN[1], GEOFFREY ELY[1]

[1] Temblor, Inc., Redwood City, CA, USA 94062
[2] Scientist Emeritus, U.S. Geological Survey; and Adjunct Professor of Geophysics, Stanford University

Temblor quantifies earthquake risk and offers solutions by connecting users with qualified retrofit and insurance providers. Temblor's weekly articles on current earthquakes, seismic swarms, eruptions, floods, and landslides makes the science accessible to the public. Temblor is available on iPhone, Android, and mobile web app platforms (http://temblor.net).

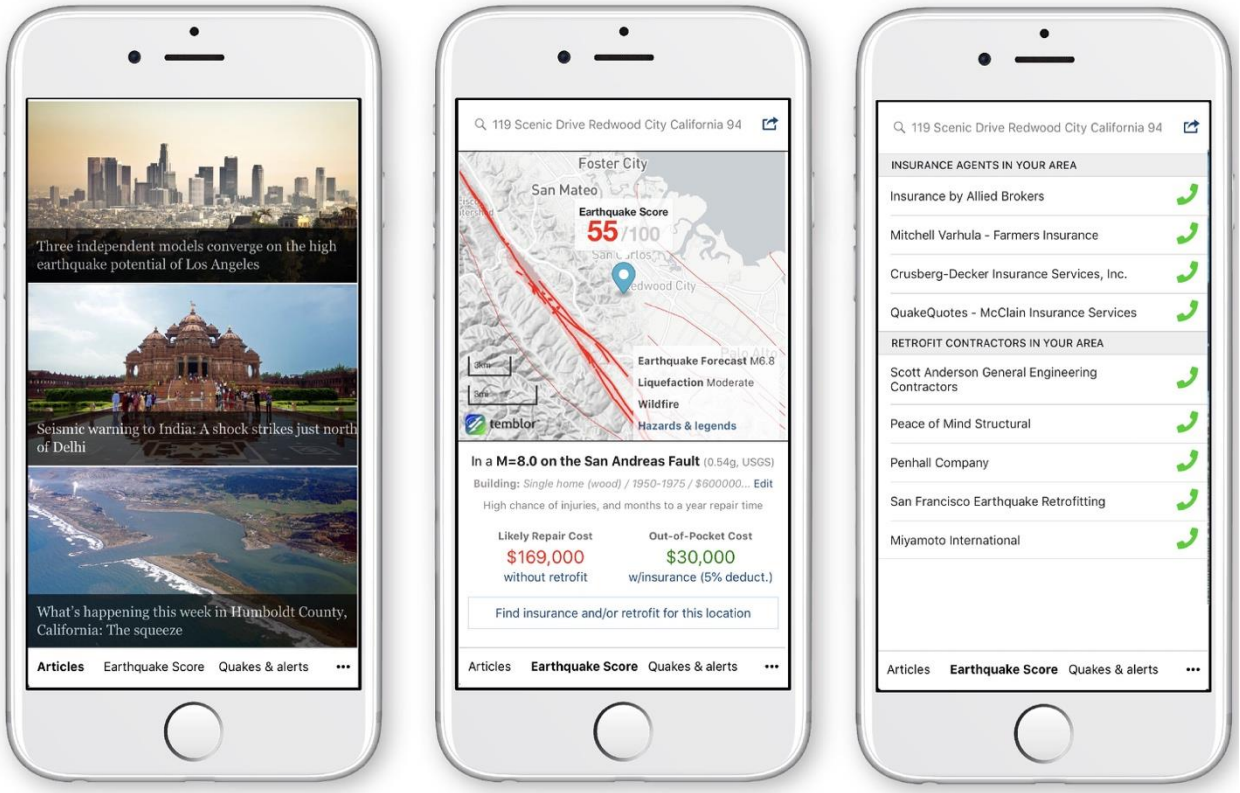

Our goal is to give the public the best estimate of their personal earthquake consequences, without scaring or soothing them. Both scenario (worst case) and probabilistic (most likely) financial losses are presented for homes and commercial buildings, with the impact of seismic retrofit and insurance on the losses and safety estimated. Temblor's map interface has clickable earthquakes and active faults around the world, and layers for liquefaction, landslides, tsunami inundation, and flood zones in the U.S. The Global Earthquake Activity Rate (GEAR) model is displayed, along with active faults displayed in 75 countries. The Temblor real-time global catalog is merged from global and national catalogs, with aftershocks discriminated from mainshocks.

Launched in 2015, Temblor has had 2.8 million session, including 15 million outside the U.S., as well as 63,000 Facebook followers and 32,000 twitter followers. All data shown in Temblor is gathered from authoritative or published sources, and combined to be intuitive, understandable, and actionable to the public. Principal data sources include USGS, FEMA, EMSC, GEM Foundation, NOAA, G-EVER, JMA, NIED, GNS Science, INGV, PHIVOLCS, and California Geological Survey and other state geological surveys.

Poster presentations

Poster list

No.	Name (First, Middle, Last)	Title
P-1	Kana Amano	Estimation of water contents at the surface of C-complex asteroids using remote sensing observations
P-2	Geri Agroli	Indication of rapid decompression induced explosive event during fluid ascent on Porphyry Copper Deposit
P-3	Serena Dominijanni	Probing the fo_2 variation in laser heated DAC experiments
P-4	Lisa Eberhard	The role of $f(O_2)$ on the stability of serpentinites in subduction zones
P-5	Wakana Fujita	Grain growth-induced fluid localization and permeability reduction
P-6	Mizuki Iida	Influence of the interannual-scale Bering Sea ice variation on cold air outbreaks
P-7	Sara Emanuel	High-resolution calcareous nannofossil biostratigraphy at Ocean Drilling Program Site 1146 in the South China Sea
P-8	Asteria S. Handayani	Geodesign Workshop 2018: an active learning implementation
P-9	Takuma Ikegaya	Hypocenter and waveform characteristics of deep low-frequency earthquakes beneath Zao volcano
P-10	Mochamad R. Iskandar	Evaluation of the water mass inside Indonesian Seas from OFES2 by lagrangian particles
P-11	Mohammad Hasib	Seismic and acoustic waves excited by volcanic explosion: analyses of energy ratio and source spectra
P-12	Takashi Hirose	Estimation of spatial changes of seismic scattering property from sparse modeling of seismic ambient noise CCFs: Application to the 2008 Iwate-Miyagi Nairiku earthquake
P-13	Enrico Marzotto	Effect of grid resolution on tectonic regimes in global-scale convection models
P-14	Caterina Melai	The conditions of sublithospheric diamond formation constrained from ferric iron-rich exsolution from ferropericlase inclusions
P-15	Yongsheng Huang	Shallow fluid circulation in mantle wedge inferred from the dihedral angle between olivine and NaCl-bearing aqueous fluid system
P-16	Ayumu Ishikawa	Source estimation of ground tilt changes associated with small explosions at Stromboli volcano
P-17	Niccolò Satta	Single crystal elasticity of Fe-bearing phase E by Brillouin spectroscopy
P-18	Marija Putak Juricek	Pargasite stability in the upper mantle at H_2O-undersaturated conditions
P-19	Mayu Kakefuda	Pb-isotope of Fe-Ni alloy associated with serpentinite: Geochemical constraints on the fluid-mediated hyper-reducing environment in mantle wedge
P-20	Kazuki Machida	Statistical correlation between tidal forces and swarm activity in the region of northern part of Wakayama Prefecture

Poster list

No.	Name (First, Middle, Last)	Title
P-21	Sando Sawa	Grain size dependency of olivine-spinel phase transformational mechanism responsible for deep-focus earthquakes
P-22	Naoko Takahashi	Incipient melting of nominally anhydrous minerals near hydrous solidus: an experimental study
P-23	Yuki Nakamura	Axisymmetric conductivities of Jupiter's middle- and low-latitude ionosphere
P-24	Theodorus Permana	Source location of volcanic earthquakes and tremors at Sakurajima volcano based on seismic correlation
P-25	Greta Rustioni	Experimental constraints on the composition of subduction zone fluids
P-26	Shunsuke Sugimura	Moment tensor inversion of very-long-period seismicity using very-near-field seismic records at Stromboli volcano
P-27	Manami Suzuki	Spatial distribution of S wave reflectors beneath the Yonezawa-Kitakata region, northeastern Japan
P-28	Miki Takahashi	Constraint for the formation temperature of the dark inclusion in a CK chondrite by thermodynamic equilibrium calculation
P-29	Naoya Takahashi	Intra-seasonal variability of oceanic low-level cloud in summertime North Pacific and its interaction with sea surface temperature
P-30	Naoya Takahashi	Variation of coseismic fault displacements on multiple seismic cycles at a site: An example from the Kamishiro fault, Itoigawa-Shizuoka Tectonic Line active fault system, central Japan
P-31	Kiriha Tanaka	Normal stress dependency of E_1' center in simulated quartz gouge by brittle fracture
P-32	Kazuya Tateiwa	Spaciotemporal change of source parameters of repeaters due to the 2011 Tohoku-Oki earthquake
P-33	Noriko Teshima	Mechanism and frequency change of pressure oscillation in the laboratory geyser system
P-34	Tong Wang	Evolutions of water mass anomalies in the upper North Pacific based on Argo data, in STMW, ESTMW, and CMW
P-35	Nao Yoshida	Seasonal and latitudinal variations of the dayside N_2/CO_2 at 140 km altitude on Mars derived from MAVEN/IUVS
P-36	Takashi Yoshizaki	The composition of the Mars
P-37	Liang Yuan	Structure of H_2O-rich Mg_2SiO_4 melts at high pressure from *ab-initio* simulations
P-38	Taku Yutani	An experimental approach to a multiple saturation point of the "direct ascent" petit-spot basalts

Poster layout (Jun. 3, Mon)

Aoba Science Hall

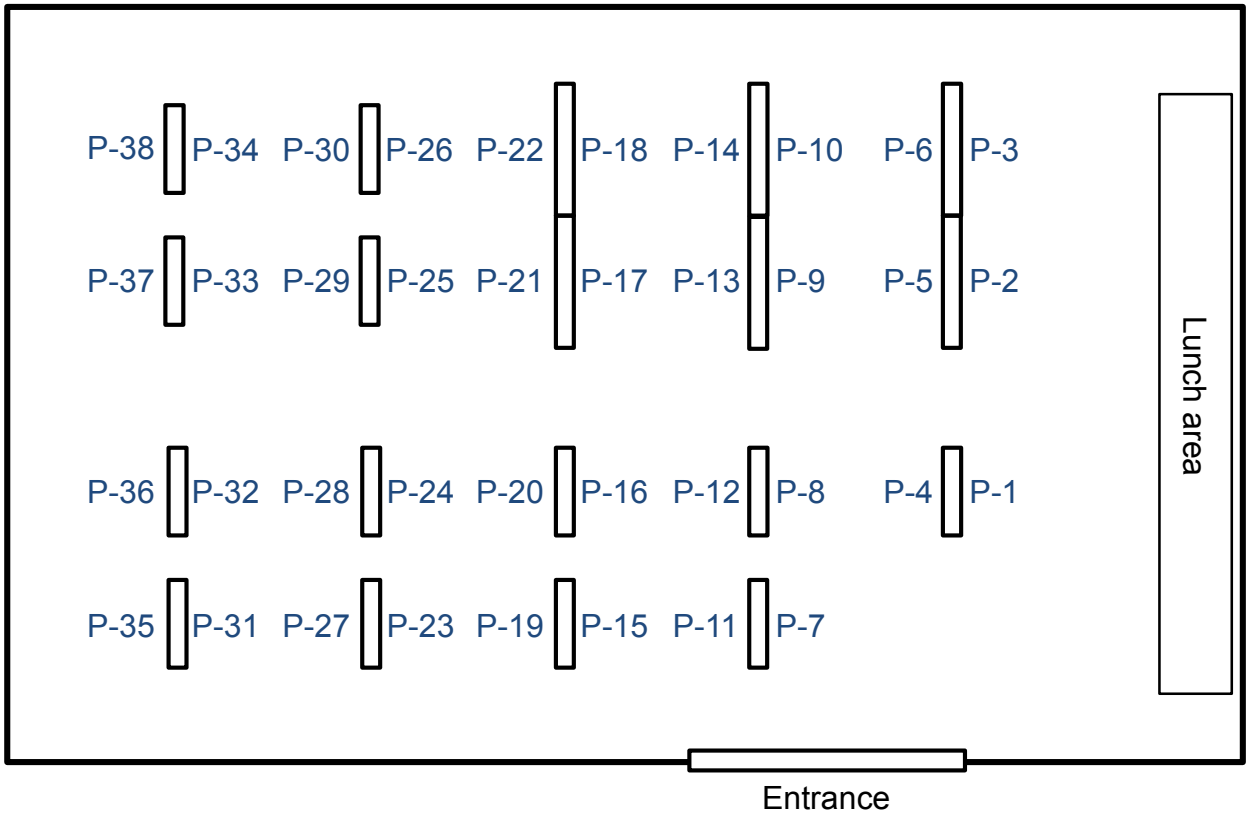

Poster layout (Jun. 4, Tue)

Aoba Science Hall

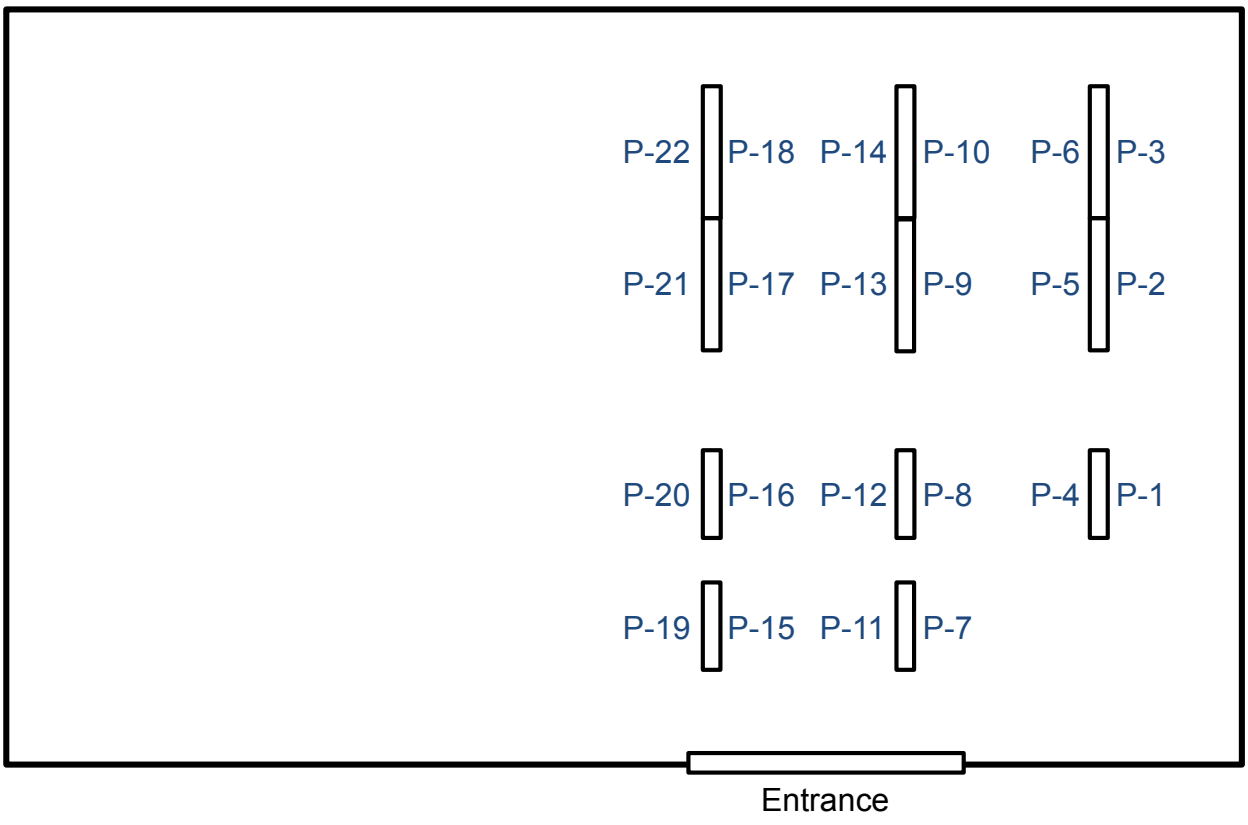

N204

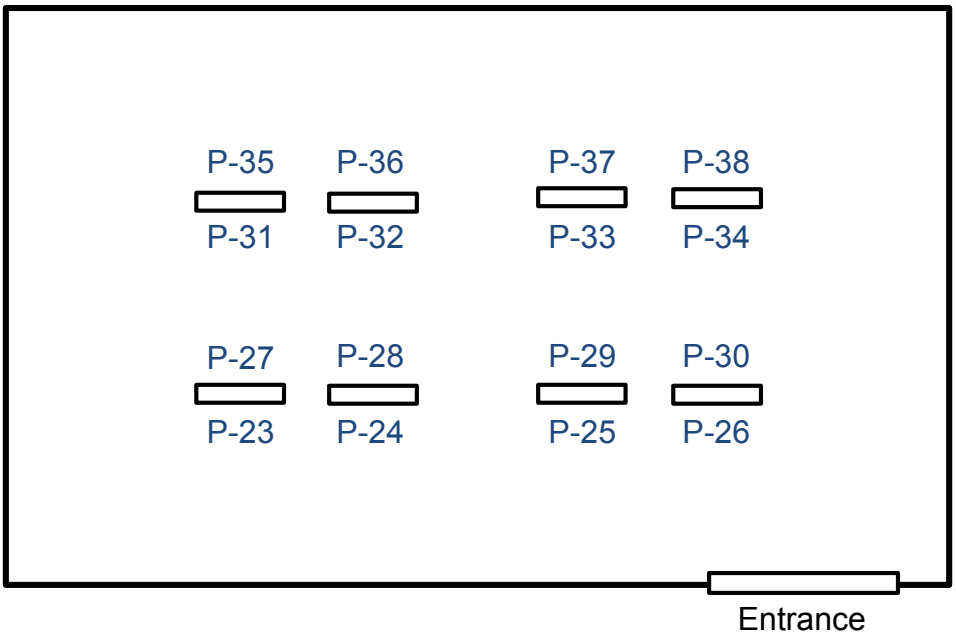

P-1

Estimation of water contents at the surface of C-complex asteroids using remote sensing observations

KANA AMANO[1], TOMOKI NAKAMURA[1]

[1] Department of Earth Science, Graduate School of Science, Tohoku University

The abundance and composition of hydrated minerals of C-complex asteroids, primitive small bodies in the solar system such as Ceres and Ryugu, reflect thermal history of them [e.g., 1]. Reflectance spectroscopy of C-complex asteroids and mineralogical study of carbonaceous chondrites, analogues of their materials, indicate heating and dehydration generally occur at the surface of them [e.g., 2-3]. Water contents of heated carbonaceous chondrites are lower than those of unheated meteorites because of dehydration of phyllosilicates [4] and experimental heating of hydrous carbonaceous chondrite Murchison weakened the strength of 3-μm band [e.g. 2-3], which indicate that heating and dehydration of the asteroids results in spectral changes and water depletion.

Although the 3-μm absorption band due to OH-stretch in hydrated minerals has been known as a direct indicator of the presence of water, ground-based observation of asteroids cannot obtain 3-μm absorption band because of telluric absorption [5]. Thus, recent observational studies using flying spectrometers [e.g., 6] have measured the 3-μm band of asteroids and revealed true forms of them in the Main Belt.

As for meteorites, recent experimental heating of fine powdery Murchison CM2 carbonaceous chondrites [7] revealed that adsorption and rehydration of atmospheric water on the heated Murchison samples severely affect the strength of the 3-μm band and the water contents. This indicates that the same water contamination occurs on the Earth to carbonaceous chondrites heated in asteroids. Therefore, spectral measurement and water analysis of heated hydrous carbonaceous chondrites without any effects of adsorbed and rehydrated water are obviously very important to compare reflectance spectra between asteroids and meteorites. In [7], experimentally heated samples were measured reflectance spectra and water contents without exposed to the air after heating. Different experimentally heated carbonaceous chondrites, Tagish Lake C2-ung and LAP 04721 CR2 [8], were analyzed by the same way in [7]. The results of these three heating experiments confirm that with increasing temperature of heating, the water content and the 3-μm band depth decrease in a similar way and they form a single trend of correlation between the water content and the 3-μm band depth regardless of their hydrated mineral composition.

The shape of the 3-μm absorption band is also affected by grain size and bulk porosity of samples. The fine-grained samples of Murchison CM carbonaceous chondrite with various grain sizes (< 77 μm to < 2000 μm) and bulk porosities (32% to 59% controlled by the number of tapping) show nearly the same peak positions of the 3-μm band, but different 3-μm band depths [9]. The results show that grain size is more effective to the depth than bulk porosity.

Particle size distributions at the surface of airless bodies might be altered by space weathering, granular transport effects, and other internal and external influences. Mean grain sizes of regolith were determined for a large number of asteroids using remote measurements of thermal inertia that depends on the heat conductivity and the volumetric heat capacity of the materials [10]. Thermal inertia of fine-grained Murchison carbonaceous chondrite with various grain sizes and bulk porosities were also measured in [9], and the detailed results will be reported in [11].

In this study, we reevaluate the relationship between the 3-μm band depth and water contents including the effects of the grain size and bulk porosity. All results taken together, this study suggests the possible way to estimate water contents taking into account the physical properties at the surface of C-complex asteroids using remote sensing.

References

[1] Jones T. D. et al. 1990. Icarus, 88, 172-192.
[2] Hiroi T. et al. 1993. Science, 261, 1016–1018.
[3] Hiroi T. et al. 1996. Meteoritics & Planetary Science, 31, 321–327.
[4] Garenne A. et al. 2014. Geochimica et Cosmochimica Acta 137, 93-112.
[5] Rivkin A. S. et al. 2002. The Astronomical Record. Asteroids III, 235.
[6] Usui F. et al. 2019. Publications of the Astronomical Society of Japan, 71, 1, 1-41.
[7] Mogi K. et al. 2017. The 80th Annual Meeting of the Meteoritical Society, Abstract #6225.
[8] Amano K. et al. 2018. The 81st Annual Meeting of the Meteoritical Society, Abstract #6309.
[9] Amano K. et al. 2019. The 20th Symposium on Planetary Sciences, #P-28.
[10] Gundlach B. and Blum J. 2013. Icarus, 223, 1, 479-492.
[11] Mita H. et al. 2019. The 82nd Annual Meeting of the Meteoritical Society, Abstract Accepted.

P-2

Indication of rapid decompression induced explosive event during fluid ascent on Porphyry Copper Deposit

GERI AGROLI[1], ATSUSHI OKAMOTO[1], NORIYOSHI TSUCHIYA[1]

[1] Department of Environmental Studies for Advanced Society, Graduate School of Environmental Studies, Tohoku University

Fluid plays an essential role in magmatic-hydrothermal processes for heat and mass transfer within the crust [1]. Fluid behavior at subsurface precipitate precious element under dynamic fluid processes [2]. Porphyry copper is one of the well-studied and best understood mineral deposit types [3]. Yet, whether internal or external factor that triggers porphyry ore-forming event is still questionable. Here, we examine quartz-bearing vein as an indicator of pore fluid fluctuation between lithostatic and hydrostatic [4] as well as calcite-quartz-cemented breccia as an indicator of high fluid flux and flow rate to ascertain decompression process that leads either to a major explosive volcano eruption or subsurface magmatic-hydrothermal event (i.e., ore formation).

700-meter drill-core obtains from Erdenet deposit, Northern Mongolia and consists of ±60 samples. Lithological facies comprise of quartz porphyry at the shallow part and granodiorite porphyry at deeper part. Three vein types recognize and exhibit truncate relationship, early qtz-mol±cal vein occurs with 2-15 mm width. Molybdenite concentrates in the edge of the vein and this vein homogenize at temperature 179.1-324°C. Ti-in-quartz geothermometer [5] record wide-range precipitation temperature at 323-678°C, suggest that this vein occurs at early fluctuation-fluid process within the porphyry system [6]. SEM-CL exhibit distinct euhedral quartz zoning. Subsequent qtz-py±ccp±cal truncate the prior vein with 3-15 mm width, this vein type homogenize at temperature 147.8-358.9°C. SEM-CL reveal vast amount of CL-dark that interconnected and create cobweb texture as indication of intense re-crystallization process and last qtz±cal has 10-15mm width and homogenize at temperature 108.6-243.3°C. CL-image show quartz within the vein as individual grain with less CL-dark was observed. The distinctive breccia texture was observed in the middle and deeper part of the core section. Breccia occurs within 1-4 cm quart-calcite-cemented vein. Clast in the breccia includes a fragment of wall-rock and the size gradually decrease with respect to vein-wall up to ±0.9mm yet no clast size smaller than this. None of the fragment is in contact with neighbors, floating-like texture indicated that high fluid flux was injected from a fluid source into the system [7].

References

[1] Bredehoeft, J. D., and Norton, D. L. (1990). The Role of Fluids in Crustal Processes. National Academy Press, 170.
[2] Weis, P., Driesner, T., & Heinrich, C. A. (2012). Porphyry-copper ore shells form at stable pressure-temperature fronts within dynamic fluid plumes. Science, 338(6114), 1613-1616.
[3] Richards, J. P. (2018). A shake-up in the porphyry world?. Economic geology, 113(6), 1225-1233.
[4] Fournier, R. O. (1999). Hydrothermal processes related to movement of fluid from plastic into brittle rock in the magmatic-epithermal environment. Economic Geology, 94(8), 1193-1211.
[5] Huang, R., & Audétat, A. (2012). The titanium-in-quartz (TitaniQ) thermobarometer: A critical examination and re-calibration. Geochimica et Cosmochimica Acta, 84, 75-89.
[6] Rusk, B., & Reed, M. (2002). Scanning electron microscope–cathodoluminescence analysis of quartz reveals complex growth histories in veins from the Butte porphyry copper deposit, Montana. Geology, 30(8), 727-730.
[7] Cox, S. F., & Munroe, S. M. (2016). Breccia formation by particle fluidization in fault zones: Implications for transitory, rupture-controlled fluid flow regimes in hydrothermal systems. American Journal of Science, 316(3), 241-278.

P-3

Probing the fo_2 variation in laser heated DAC experiments

SERENA DOMINIJANNI[1], CATHERINE A. MCCAMMON[1], LEONID DUBROVINSKY[1], DANIEL J. FROST[1], NOBUYOSHI MIYAJIMA[1], TIZIANA BOFFA-BALLARAN[1]

[1] Bayerisches Geoinstitut, University of Bayreuth, Germany

The distribution and circulation of oxygen in the Earth's interior strongly controls the redox state of the mantle that affects the global geodynamic cycle of the volatile elements. Understanding the oxygen fugacity (fo_2) conditions of the Earth's mantle is a crucial issue since it exerts a first order control on subduction, convection, partial melting and metasomatism processes as well as on the minerals phase equilibria. Laser heated diamond anvil cell (DAC) experiments allow us to reach high pressures and temperatures conditions of the deep Earth's interior. However, so far the redox conditions during diamond anvil cell (DAC) experiments have never been constrain.

Adopting the redox sensor approach, we investigated the fo_2 variation during DAC experiments using a mixture of synthetic ferropericlase $(Mg_{0.75}Fe_{0.25})O$ and pure Ir powder in order to crystallize an Fe-Ir alloy and use it to calculate the oxygen fugacity. Double side laser heating experiments were performed employing piston-cylinder type BX90 diamond anvil cells at ID15b, ID27 and ID18 beamlines of the European Synchrotron Radiation Facility (Grenoble, France) where powder X-ray diffraction (XRD) and Synchrotron Mössbauer Source (SMS) data have been collected. After recovering, the samples were chemically characterized using the Energy-Dispersive X-ray Spectroscopy (EDS) and the Electron Energy Loss Spectroscopy (EELS) at Bayerisches Geoinstitut (Bayreuth, Germany).

Preliminary results from powder X-ray diffraction data show that, after heating, an Fe-Ir metal alloy that can be indexed in the Fm-3m space group is formed by the reaction of pure Ir and Fe from ferropericlase according to the reaction:

$$(Mg,Fe)O + Ir \rightarrow (Mg,Fe)O + (Fe,Ir)$$

The compressibility of the Fe-Ir alloy and ferropericlase was measured up to ~ 60 GPa and SMS data were collected before and after heating. X-ray diffraction results coupled with energy-dispersive X-ray spectroscopy (EDS) measurements and a simple thermodynamic model indicate that the redox conditions during the DAC experiments were close to the iron-wüstite (IW) buffer, although some inhomogeneity was observed. Further chemical analyses and additional experiments are ongoing to understand the variation of oxygen fugacity in a DAC during laser heating.

P-4

The role of $f(O_2)$ on the stability of serpentinites in subduction zones

LISA EBERHARD[1], DAN FROST[1]

[1] Bavarian Research Institute of Experimental Geochemistry and Geophysics, BGI

Serpentinite minerals are 1:1 trioctahedral phyllosilicates and the most abundant phase in hydrated oceanic crust. They cover a wide compositional range in terms of Al content, total Fe content, and $Fe^{3+}/\Sigma Fe$ ratio and are the main water carriers in subduction zones containing up to 13wt% H_2O.

The stability of serpentinites as a function of P and T is subject of many field and experimental studies. Differences in dehydration temperature at a fixed pressure are often interpreted as a result of composition. It is suggested that Al has a positive effect on the stability of serpentinite minerals at dehydration depth, whereas total Fe content shows the opposite effect. Nevertheless, comparing literature data these effects can only account for some differences and additional discrepancies still exist.

In this study the stability of serpentinites has been reanalyzed as a function of $f(O_2)$ in multi-anvil experiments. Natural serpentinites mainly composed of antigorite are used as starting materials with initially high and low Fe^{3+}/Σ Fe ratios. Experiments were performed over a range of oxygen fugacities for approximately 3 days over the stability field of serpentinite minerals. Additional experiments were performed on serpentinite+carbonate mixture in order to also identify possible effects of carbon on the serpentinite stability. Run products were examined using the electron microprobe and the Fe^{3+}/Σ Fe ratios were determined using Mössbauer spectroscopy.

We find a minor effect of Fe^{3+} content on the stability of antigorite. Comparison with literature data and recent field studies support our finding that ferric Fe stabilises the serpentinite phase. However, we also determine the relationship between the Fe^{3+}/Σ Fe ratio of serpentine and the oxygen fugacity. Antigorite Fe^{3+}/Σ Fe ratios are found to decrease sharply at a constant oxygen fugacity as dehydration commences. This means that in a subducting assemblage where a constant Fe^{3+}/Σ Fe ratio is maintained the oxygen fugacity must increase as antigorite dehydration occurs. This will have important implications for the speciation of variable valent elements in subducting slabs such as carbon and sulphur.

P-5

Grain growth-induced fluid localization and permeability reduction

WAKANA FUJITA[1], MICHIHIKO NAKAMURA[1], KENTARO UESUGI[2]

[1] Department of Earth Science, Graduate School of Science, Tohoku University, Japan
[2] Synchrotron Radiation Research Institute (JASRI/SPring-8)

Efficiency of segregation of geological fluids such as aqueous fluids and melts is an essential concept for volatile cycles in subduction zones. Permeability is an intrinsic rock property that controls flow rate of fluid. Various permeability models have been presented by numerical models of textually equilibrated rocks [1,2], laboratory measurements on synthetic rocks [3] and estimation from cross-sectional area of synthetic rocks [4]. However, there exist discrepancies among those models. Because permeability is very sensitive to microscopic geometry of pore fluid, those disagreements arise from lack of understanding toward three-dimensional (3D) microstructure of fluid network.

Dihedral angle has been considered to be a critical parameter that controls fluid geometry and thus permeability. Some previous studies shed light on effect of grain growth on fluid distribution because it could induce pore fluid distortion and coalescence [5,6]. These studies suggest that in the actual systems where the microstructure of rocks evolve in dynamic processes, grain growth would be rather important than the dihedral angle.

To investigate the effect of grain growth on the fluid distribution and permeability, we present 3D images of quartz–CHO fluid aggregates, containing nominal fluid fractions between 0.03 and 0.10. Samples were synthesized from a powdered mixture of Arkansus quartz and amorphous silica prepared by sol-gel method and hot-pressed in a piston–cylinder apparatus at 900°C and 1.0 GPa for 192h. The fluid fractions and the dihedral angles were controlled using brucite added in the capsule bottom and oxalic acid dihydrate mixed with SiO_2 powder. 3D images were obtained using synchrotron X-ray microtomography at BL20XU experimental hutch2 of Spring-8. Regardless of dihedral angles (CO_2 content in fluids), both cross-sectional area and 3D images of samples showed grain-scale fluid localization which would be formed by pore fluid coalescence induced by grain growth. Computed permeabilities using numerical model, LaMEM (Lithospheric and Mantle Evolution Model [7]) were almost consistent with laboratory measurements by [3] but more than one order of magnitude lower than a numerical model by [2]. This would indicate that localized fluids extensively reduce permeability by reducing the diameter of fluid tubes along grain edges, which would suggest water transport into Earth's deep interior.

References

[1] von Bargen N, Waff, H.S. 1986, J. Geophys. Res. 91, 9261–9276.
[2] Rudge, J.F. 2018, Proc. R. Soc. Lond. A 474, 20170639.
[3] Wark, D. A., Watson, E. B. 1998, Earth Planet. Sci. Lett. 164, 591–605.
[4] Faul, U.H. 1997, J. Geophys. Res. 102, 10299–10311.
[5] Walte, N. P., Bons, P. D., Cees, W., Passchier, Koehn, D. 2003, Geology 2003 31, 1009-1012.
[6] Yoshino, T., Watson, E. B. 2005, Earth Planet. Sci. Lett. 235, 453–468.
[7] Kaus, B. J. P., Popov, A. A., Baumann, T. S., Püsök, A. E., Bauville, A., Fernandez, N., Collignon, N. 2016, NIC Symposium 2016

P-6

Influence of the interannual-scale Bering Sea ice variation on cold air outbreaks

MIZUKI IIDA[1], SHUSAKU SUGIMOTO[1], TOSHIO SUGA[1]

[1] Department of Geophysics, Graduate School of Science, Tohoku University

In the Northern Hemisphere winter, cold air outbreaks occur over East Asia and the eastern North America. Quantitative estimation of a cold air mass was developed recently and this allowed us to detect two climatological cold air streams (Iwasaki et al., 2014 [1]): the East Asian stream and the North American stream. Cold air incursions are strongly affected by the terrain and land–sea distributions, and the cold air mass is lost due to diabatic heating over the northwestern parts of the North Pacific and the North Atlantic, which are downstream regions of the two streams (Kanno et al., 2015 [2]). The East Asian stream passes over the Bering Sea covered by ice. It is expected that the Bering Sea ice would affect the path and formation/loss of cold air mass. However, the influence of sea ice, including the Bering Sea, on the cold air mass has been unclear. We investigate a temporal relationship between the Bering Sea ice and the cold air mass and discuss its cause from the view point of large-scale atmosphere patterns, by applying statistical methods. In addition, we try to describe an influence of cold air mass on ocean mixed layer temperature and depth. Following a pioneering work by Iwasaki et al. (2014) [1], we calculate negative heat content (NHC), which is regarded as a cold air mass amount below potential temperature of 280K, by using ERA-Interim data. We use the Bering Sea ice concentration from NOAA OISST v2 dataset. Analysis period is 37 years of 1982-2018, and we focus on February because the Bering Sea ice concentration has the largest value and the largest variance. In order to extract the NHC and atmosphere patterns related to the Bering Sea ice variation, we perform a composite analysis. Here, we define two categories (high and low ice concentration years) based on the regional time series of Bering Sea ice concentration (160°E-150°W, 55°N-65°N); high (low) ice concentration years are defined as years in which sea ice concentration is above (below) plus (minus) one standard deviation from the long-term mean. In high ice concentration years, NHC is found in the Bering Sea and the Bering Strait, showing southward NHC flux. NHC loss is dominated over a region south of the Bering Sea. Composite maps of sea level pressure and geopotential height show remarkably large amplitude in the central North Pacific, indicating a change of the Aleutian Low intensity. We checked a relationship between the Bering Sea ice concentration and large-scale atmospheric patterns such as Pacific/North Atlantic pattern, West Pacific pattern, and El Nino. Interestingly, the Bering Sea ice concentration is not significantly correlated with climate indices representing the atmosphere patterns mentioned above. Our result implies that the Bering Sea ice concentration has a potential to affect the cold air mass outbreak and the NHC. In the presentation, we introduce an impact of the NHC loss on the underlying ocean.

References

[1] Iwasaki, T., T. Shoji, Y. Kanno, M. Sawada, M. Ujiie, and K. Takaya (2014), Isentropic analysis of polar cold air mass streams in the northern hemispheric winter, J. Atmos. Sci., 71(6), 2230–2243

[2] Kanno, Y., M. R. Abdillah, and T. Iwasaki (2015), Charge and discharge of polar cold air mass in northern hemispheric winter, Geophysical Research Letters, 42, 7187-7193

P-7

High-resolution calcareous nannofossil biostratigraphy at Ocean Drilling Program Site 1146 in the South China Sea

SARA EMANUEL[1], TOKIYUKI SATO[2], SHUN CHIYONOBU[2], YASUFUMI IRYU[1]

[1] Department of Earth Science, Graduate School of Science, Tohoku University
[2] Faculty of International Resources Sciences, Akita University

The South China Sea (SCS) is the largest marginal sea in the western Pacific. Tectonically, the SCS is bounded by Indochina Block on the west, Philippines Sea plate on the east and Yangtze Block to the north. The formation of the South China Sea basin was closely related with the collision between the Indian Plate and Eurasian Plates. The SCS underwent five tectonic evolution stages: rift system development, sea floor spreading, subsidence of the South China Sea, closure of the South China Sea Basin, and uplift of Taiwan. Based on the drifting history of the Indian, Australian, and Pacific plates since the Cretaceous, it suggested that the initiation of the SCS was controlled by backarc extension associated with the northward subduction of the Neotethys. The variability of East Asian winter monsoon (EAWM) has been linked closely to the rise and decline of the Northern Hemisphere ice sheets (NHIS) through the Siberian High over the last 2.8 Myr. Geochemical and foraminiferal data from ODP sites 1143 and 1146 suggest that the mean state of super El Niño–Southern Oscillation (ENSO) is strongly modulated the EAWM strength through remote forcing to generate the 400 kyr cycle between 2.8 Ma and 1.2 Ma, while the low NHIS volume was not sufficient to dominate the EAWM variation. In contrast, the high NHIS volume has controlled the EAWM variation for the last 0.9 Myr with 100 kyr cycles. All biomarker contents indicate higher individual and total phytoplankton productivities during peak glacials than during interglacials. The spatial pattern of productivity in glacial periods suggest that its increases in the southeastern and northern SCS were caused by the stronger East Asian winter monsoon (EAWM), which brought more nutrients to the sea surface through stronger inputs of nutrient-rich deep waters. Therefore, the South China Sea (SCS) is an ideal field to study biotic responses to orbitally controlled climate changes during the late Cenozoic.

This study presents the first high-resolution calcareous nannofossil biostratigraphy in the South China Sea (SCS). A total of 306 samples from ODP Site 1146 (19°27.40′N, 116°16.37′E) were analyzed. The studied sediments are late Pliocene to Quaternary in age. Microscope slides were prepared following Imai et al. (2013) [1]. The slides were observed under a binocular polarizing microscope with an oil-immersion objective lens at a magnification of x1000. Forty-five species coming under 25 genera were identified. A total of 14 calcareous nannofossil datums were found. The datums of this study were defined based on the First Occurrence (FO) and Last Occurrence (LO) of the age-diagnostic species. The detected datums were: FO *Emiliania huxleyi* (0.265 Ma), LO *Pseudoemiliania lacunose* (0.451 Ma), LO *Reticulofenestra asanoi* (0.853 Ma), FO *Gephyrocapsa parallela* (0.987 Ma), FO *Reticulofenestra asanoi* (1.128 Ma), LO *Gepyrocapsa* spp. (large) (1.182 Ma), FO *Gephyrocapsa* spp. (large) (1.392 Ma), FO *G. oceanica* (1.706 Ma), FO *G. caribbeanica* (1.763 Ma), LO *Discoaster brouweri* (1.990 Ma), LO *D. pentaradiatus* (2.424 Ma), LO *D. surculus* (2.487 Ma), LO *D. tamalis* (2.721) and LO *R. ampla* (2.743 Ma). The LO *Helicosphaera sellii* (1.219 Ma) which was supposed to be in between FO and LO *Gephyrocapsa* spp. (large) could not be detected since the specie is rarely and sporadically present in the lower Pleistocene and Pliocene interval at the studied site. The LO *D. brouweri* was difficult to find because reworked coccoliths of this species were common in upper section. Therefore, it was determined as a horizon at which the relative abundance of this species exceeded 2%.

References

[1] Imai, R., Sato, T., & Iryu, Y. (2013). Chronological and paleoceanographic constraints of Miocene to Pliocene 'Mud Sea' in the R yukyu Islands (southwestern Japan) based on calcareous nannofossil assemblages. *Island Arc, 22*(4), 522-537.

P-8

Geodesign Workshop 2018: an active learning implementation

ASTERIA S. HANDAYANI[1], YUZURU ISODA[1]

[1] Department of Earth Science, Graduate School of Science, Tohoku University

Tohoku University has strived to put the policy of 'practice-oriented research and education' into its educational system, to develop cultured human resources with deeply specialized knowledge and contributions to solution of various kinds of social issues, particularly the ones which related with the Earth Science. In the process, the importance of having an active learning environment has been reinforced, as a positive way forward to make students enjoy their lessons more and understand better. Evaluation of common misconceptions, e.g.: (1) lecture-based methods of teaching, (2) concern whether to give students the freedom to solve problems by themselves, has been conducted as well.

In view of this, a Geodesign Workshop held by Human Geography research group of Tohoku University Graduate School of Science, Earth Science Department from October to December 2018 could be considered as one of the evidence of the active learning approach implementation. The Workshop, which integrated multiple disciplines and used geographical information systems (GIS)-based analytic and design tools, was participated by around twenty-five international undergraduate and graduate students from six different countries. Taking the theme of Alternative Future of Sendai in 2050, the Workshop invited participants to imagine, evaluate, and design the ideal future for sustainable Sendai City by analyzing and sharing their ideas in teams, based on ten development issues (i.e, water, agriculture, green infrastructure, natural hazards, industry and distribution, energy infrastructure, transport infrastructure, residential, institutional uses, and mixed-use development) which should be considered by policymakers. During the Workshop, the professor acted as a facilitator rather than a teacher. An evidence to the effectiveness of the practice, the Workshop changed the beliefs and values of the participants. Prior to the Workshop, majority of participants did not believe Sendai City will expand further, but most were convinced that it will, after the Workshop. Simultaneously, majority of participants believed compact city is ideal for the city beforehand, but half of them changed their minds that the city may expand given financial and political cost of making a city compact. As a result, the teams developed ten evaluation maps and three final design maps by working responsibly and collaboratively, given the freedom to think and plan for a better future. The outcome was submitted to International Geodesign Collaboration Meeting 2019, 23-25 Feb 2019, Redlands (CA), where over 90 universities world-wide done similar workshop for their own areas (https://docs.wixstatic.com/ugd/f24d78_df9e732211b34ffa9d4b8caca5b3d626.pdf). In conclusion, this kind of teaching method in cross-cutting issues in earth science issues with urban planning have proven to be effectively engaged students to enjoy their learning time at the University and make contribution for society.

Keywords: active learning; cross-cutting issues; geodesign; workshop

P-9

Hypocenter and waveform characteristics of deep low-frequency earthquakes beneath Zao volcano

TAKUMA IKEGAYA[1], MARE YAMAMOTO[1]

[1] Department of Geophysics, Graduate School of Science, Tohoku University

The 2011 Tohoku Earthquake (Mw 9.0) caused large crustal deformation in and around the Tohoku region, and strongly affected volcanic fluid in the crust. As an example suggesting such influence, the change in activities of deep low-frequency earthquakes (DLFs) occurring in the lower crust has been observed at several volcanoes in Tohoku region after the earthquake. The analysis of DLFs is thus considered to be one of the important keys to infer the activity of deep magma and to assess the potential risks of mid- to long-term volcanic activity after a huge earthquake. In this presentation, we report the results of our analysis of the DLFs beneath Zao volcano where activation of volcanic activities has been observed after the 2011 Tohoku Earthquake.

Zao volcano is located on the border between Yamagata and Miyagi prefectures. After the 2011 Tohoku Earthquake, the number of DLFs beneath Zao volcano started increasing, and increase in shallow seismicity have been observed since 2013. Though the JMA unified hypocenter catalog (JMA catalog) is often used for investigating such seismic activities, the completeness of the catalog is not guaranteed in small DLFs. To improve the completeness of event detection and understand the detailed spatio-temporal characteristics of DLF activity, we apply Matched Filter method (MF method) to the waveform data for the last seven years, and determine relative hypocenters of the detected DLFs.

In the analysis, we used the continuous three-components waveform data recorded at four permanent stations operated by Tohoku Univ., NIED, and JMA. 146 DLFs listed in JMA catalog between Jan. 2012 and Sept. 2016 were selected as templates for the MF analysis. We used a frequency band of 1-8 Hz and set the detection threshold to 0.2. The time windows exceeding the threshold were visually checked to eliminate false detections. For each detected DLFs, using cross spectrum and correlation functions, we estimated the differential travel times between the detected DLF and the template having maximum correlation, and determined the relative hypocenter using the master event method.

As a result, we detected 1361 DLFs between Jan. 2012 to May 2018, which is about 10 times the number of templates, and determined 1357 hypocenters whose spatial distribution shows two clusters above and below 28 km. We also checked the individual waveforms of the detected DLFs to understand the nature of spatial clustering of DLFs, and revealed that DLFs can be classified into the following two types in a large sense: the first type (354 events) shows high-frequency (4-8 Hz) component in the initial part (1-2 s) of the waveform, and low-frequency (1-4 Hz) component in the remaining part of the waveform; the second type (1007 events) shows low-frequency (1-4 Hz) component over the entire waveform. The depth distribution of the former type has a peak around 33 km and widely spreads (20-38 km) whereas that of the latter type is confined within a narrow range (20-26 km). These results suggest that source processes of DLFs differ between the two clusters above and below 28 km. On the other hand, there is no clear difference in the Gutenberg-Richter law *b* values of both types.

Our further analysis including estimation of the source mechanisms of the detected DLFs may contribute to the understanding of the distribution and activities of deep volcanic fluid.

P-10

Evaluation of the water mass inside Indonesian Seas from OFES2 by Lagrangian particles

ISKANDAR MR[1], YANLI JIA[2], HIDEHARU SASAKI[3], TOSHIO SUGA[1], KELVIN RICHARDS[2]

[1] Department of Geophysics, Graduate School of Science, Tohoku University
[2] International Pacific Research Center, University of Hawaii
[3] Application Laboratory, JAMSTEC

Indonesian Seas are known as the region of enhanced vertical mixing. The tidal mixing is considered as a contributor to changes the water mass properties within the Indonesian area. Ocean model data from JAMSTEC (OGCM for the Earth Simulator, OFES) has been improved recently using tidal scheme implementation, called OFES2. The increase of ITF transport by internal tidal mixing in OFES2 have been reported. However, the water mass properties in the Indonesian region in OFES2 have not been described yet. Here, we use Lagrangian analysis by releasing particles at Makassar Strait and Lifamatola Strait to analyze the water mass properties along the western and eastern route of ITF. The examination of the spatial distribution of vertical diffusivity in OFES2 along the pathways of ITF would identify where tidal mixing is still lacking. The comparison of water mass properties in OFES1 and OFES2 with observations (WOD13/LIPI) in the Indonesian Seas shows that tidal mixing brings OFES2 closer to observation, but substantial regional differences remain. It is shown that the vertical diffusivity is quite low in the Sulawesi Sea resulting in the similar TS properties downward to Makassar Strait. Particularly in the eastern route region, the vertical diffusivity in Lifamatola Strait is low, suggesting the mixing is not strong enough to erode the high salinity subtropical water downward. Along particle pathway, the high vertical mixing occurs in small channel (i.e. Labani channel) or the boundary (i.e. Sibutu passages in northern Sulawesi boundary or along New guinea coast). In the western route, suggesting there is lack of mixing in the Sulawesi Sea. While the Kv is very large. In the eastern route, the water mass is quite good even with smaller Kv than western route. Still need to answer why high Kv can't erode the high salinity water in Sulawesi Sea.

References

[1] Sasaki, H., Kida, S., Furue, R., Nonaka, M., & Masumoto, Y. (2018). An Increase of the Indonesian Throughflow by Internal Tidal Mixing in a High-Resolution Quasi-Global Ocean Simulation. *Geophysical Research Letters, 45*(16), 8416-8424. doi:doi:10.1029/2018GL078040

[2] Sebille, E., England, M. H., Zika, J. D., & Sloyan, B. M. (2012). Tasman leakage in a fine-resolution ocean model. *Geophysical Research Letters, 39*(6). doi:doi:10.1029/2012GL051004

[3] Koch-Larrouy, A., Madec, G., Blanke, B., & Molcard, R. (2008). Water mass transformation along the Indonesian throughflow in an OGCM. *Ocean Dynamics, 58*(3), 289-309. doi:10.1007/s10236-008-0155-4

P-11

Seismic and acoustic waves excited by volcanic explosion: analyses of energy ratio and source spectra

MOHAMMAD HASIB[1], TAKESHI NISHIMURA[1], HISASHI NAKAHARA[1]

[1] Department of Geophysics, Graduate School of Science, Tohoku University

Volcanic eruptions generally accompany both seismic and acoustic signals, and these signals are used to understand the volcanic fluid motions in the conduit and/or its effusion process from active vents. In the present study, we compare these two kinds of signals observed at several volcanoes in Japan, systematically examining the temporal changes of radiation energy. We further examine the basic spectral characteristics of seismic and acoustic signal radiations during large and small Vulcanian explosion at Sakurajima volcano. We use seismic and acoustic records at seismic-acoustic stations operated by Japan Meteorological Agency (JMA).

We first examine the energy ratio between seismic and acoustic signal of volcanic explosion at Sakurajima, Kirishima, and Kuchinoerabu-jima volcano. We calculate the time series of energy ratio of acoustic signal to three component seismic signals by calculating their envelopes at the frequency bands of 1-5 Hz. To obtain averaged characteristics, we stack the energy ratios of seismic and acoustic signals of about 265 explosions at Sakurajima and 9 explosions Shinmoe-dake (Kirishima) volcanoes, respectively. We analyze only one eruption at Kuchinoerabu-jima. Analyses of about 265 explosions at Sakurajima and about 5 explosions at Shinmoedake (Kirishima) show the following characteristics in the temporal changes of energy ratios of seismic to acoustic signals at the all frequency ranges: the ratio of seismic energy to acoustic energies rapidly decreases at the beginning, and reach the minimum for about 10 s -20 s; then the ratio gradually increases for 20 s - 40 s; the seismic signals continue after the acoustic energy decreases down to the noise level. Although we can analyze one eruption data for Kuchinoerabu-jima volcano (18 December 2018), similar characteristics are recognized. These results suggest that the volcanic fluid motions are strong in the shallow parts in the beginning, and the active zone gradually becomes deep.

Next, we investigate the source spectra of acoustic signals of volcanic explosions. Applying the spectral ratio method that has been often used for seismic signals, we clarify the difference of source spectra between large and small acoustic signals. We stack the spectral ratios of acoustic signals according to their maximum amplitudes, and classify them into Classes IV, III, II, and I from the largest to the smallest. The maximum amplitude of the largest event is about 10 Pa, while the smallest is about 2.5 Pa. Since the wind around the craters and volcanoes may disturb the wave propagations, we only select the acoustic signals excited by volcanic explosion during low wind speed (< 3.3 m/s) condition, using the assimilation wind data recorded by ECMWF (European Centre for Medium-Range Weather Forecasts). We observe that the spectral ratios of acoustic signals at different stations are similar to each other both for direct and coda waves. This means that the spectral ratio method is applicable for the acoustic signals of volcanic explosions during low wind speeds. All pair of the observed source spectral ratios of acoustic signals (Class IV/I, III/I, II/I) are characterized by almost flat amplitudes at the frequency range of about 0.2 -10 Hz. The difference between the classes is the amplitude. These are observed significant for direct waves (lapse time of 5 s from the onset). This characteristic is much different from the seismic signals excited by Vulcanian explosions (Hasib et al., 2018), in which a flat amplitude at low frequency range (about 0.5 - 2 Hz), a gradual decrease with frequency at an intermediate frequency range (about 2– 3.5 Hz), and a flat amplitude at high frequency range (about 3.5 –10 Hz). These differences suggest the differences in the generation mechanisms between seismic and acoustic signals, which may reflect the difference of excitation region: the seismic waves are in the volcanic conduit beneath the vent, while the acoustic waves are at the orifice of the conduit.

Keyword: Acoustic wave, seismic wave, energy ratio, source spectra, volcanic explosion.

Acknowledgements: We used JMA seismic and acoustic signal records.

P-12

Estimation of spatial changes of seismic scattering property from sparse modeling of seismic ambient noise CCFs: Application to the 2008 Iwate-Miyagi Nairiku earthquake

TAKASHI HIROSE[1], HISASHI NAKAHARA[1], TAKESHI NISHIMURA[1], MICHEL CAMPILLO[2]

[1] Department of Geophysics, Graduate School of Science, Tohoku University
[2] University Grenoble Alpes, CNRS, ISTerre

In recent years, spatial distributions of seismic velocity and/or seismic scattering property changes associated with volcanic activities and earthquakes have been investigated by linear least-squares inversions using seismic ambient noise cross-correlation functions (CCFs) and sensitivity kernels (e.g., [1,2]). However, spatial distributions of medium changes are not easily estimated in the regions where only a small number of stations are set up. Here, we use sparse modeling (L1 norm regularization) to estimate model parameters for a small data set (e.g., [3]), and evaluate the minimum number of stations for these studies. We apply the sparse modeling to the 2008 Mw 6.9 Iwate-Miyagi Nairiku earthquake that occurred on 14 June 2008, and estimate the spatial distribution of seismic scattering property changes from decoherence (waveform changes) data of seismic ambient noise CCFs. Since we have enough seismic stations, we can compare the results from the sparse modeling and those from an ordinary linear least-squares inversion with L2 norm regularization which has been widely used to solve linearized problems.

Seismic ambient noise CCFs were calculated at 0.5-1 Hz band for the pairs among 17 Hi-net stations during the years of 2007 and 2008. We firstly calculate decoherence values between reference CCFs (Jan-Dec, 2007) and target CCFs in two time periods of May 1 to June 13 (Period I) and June 15 to July 31 (Period II) in 2008, respectively. We then calculate the differences of decoherence values of Period I and Period II, and use them as observed decoherences. Totally, 450 observed decoherence values are analyzed. Finally, we divide the study area into 63 small cells with a size of 0.15°× 0.15° and estimated scattering coefficient changes, Δg, for each small cell by comparing the observed and synthesized decoherence values. Here, we estimate synthesized decoherence values using 2-D decorrelation kernels [4].

The result from the linear least-squares inversion with L2 norm regularization shows that large Δg values are estimated around the epicenter of the main shock. The region of the largest Δg value is located at the south of the epicenter also from the sparse modeling. The maximum Δg value is about 0.029 km^{-1}, which is almost equivalent to the total scattering coefficient at this region. To know a minimum number of stations for the estimation, we selected the stations, and conducted the same estimations using the sparse modeling. We confirmed that 5 stations were necessary to recover the similar result.

The regions with large Δg values are well correlated with the region where large peak ground acceleration and large seismic velocity decreases are obtained [5,6]. This consistency suggests that strong motion by the main shock introduce not only large seismic velocity decreases but also large seismic scattering property changes in the shallow medium at the south of the epicenter. The sparse modeling will be useful to locate a change region of seismic scattering property changes from a sparse seismic network with several seismic stations.

Acknowledgements: We would like to thank the High Sensitivity Seismograph Network (Hi-net), NIED for providing the waveform data used in the present study.

References

[1] Obermann, A., T. Planès, E. Larose, and M. Campillo (2013), Imaging preeruptive and coeruptive structural and mechanical changes of a volcano with ambient seismic noise, J. Geophys. Res. Solid Earth, 118, 6285–6294, doi:10.1002/2013JB010399.
[2] Obermann, A., B. Froment, M. Campillo, E. Larose, T. Planès, B. Valette, J. H. Chen, and Q. Y. Liu (2014), Seismic noise correlations to image structural and mechanical changes associated with the Mw7.9 2008 Wenchuan earthquake, J. Geophys. Res. Solid Earth, 119, 3155–3168, doi:10.1002/2013JB010932.
[3] Tibshirani, R. (1996), Regression Shrinkage and Selection via the Lasso, Journal of the Royal Statistical Society, Series B (Methodological), 58(1), 267-288, http://www.jstor.org/stable/2346178.
[4] Margerin, L., T. Planès, J. Mayor, and M. Calvet (2016), Sensitivity kernels for coda-wave interferometry and scattering tomography: theory and numerical evaluation in two-dimensional anisotropically scattering media, Geophys. J. Int., 204, 650–666, https://doi.org/10.1093/gji/ggv470.
[5] Takagi, R., T. Okada, H. Nakahara, N. Umino, and A. Hasegawa (2012), Coseismic velocity change in and around the focal region of the 2008 Iwate‐Miyagi Nairiku earthquake, J. Geophys. Res., 117, B06315, doi:10.1029/2012JB009252.
[6] Hobiger, M., U. Wegler, K. Shiomi, and H. Nakahara (2012), Coseismic and postseismic elastic wave velocity variations caused by the 2008 Iwate-Miyagi Nairiku earthquake, Japan, J. Geophys. Res., 117, B09313, doi:10.1029/2012JB009402.

P-13

Effect of grid resolution on tectonic regimes in global-scale convection models

ENRICO MARZOTTO[1], MARCEL THIELMANN[1], GREGOR J. GOLABEK[1]

[1] Bayerisches Geoinstitut, University of Bayreuth, Bayreuth, Germany

Global-scale convection models using a visco-plastic rheology coupled with a temperature-dependent viscosity usually show different tectonic regimes: mobile, episodic or stagnant lid.

In the mobile lid regime, the lid is continuously subducting into the mantle (plate-like behavior). The episodic lid regime is characterized by the stability of the lid until sufficiently large lithospheric stresses break it, causing rapid resurfacing. Finally the stagnant lid regime is defined by an undeformable lid that does not participate in convection

In numerical simulations these three types of regimes can be obtained by varying some target parameters such as: temperature-dependency of viscosity and yield stress.

The yield stress in particular is a key parameter because it sets the stress necessary to cause plastic yielding, hence, in a visco-plastic rheology, the stress necessary to break the cold surface regions. A high yield stress will result in a stagnant lid. On the other hand, a low yield stress causes a weak lid that is constantly broken and sinks into the mantle. Despite the key importance of physical parameters, also numerical parameters have an effect on the tectonic regime, determining different outcomes just by changing the grid resolution.

Here we use the code StagYY (*Tackley, 2008* [1]) in a 2D spherical annulus geometry (*Hernlund & Tackley, 2008* [2]) to determine the resolution-dependent tectonic regime for different yield stresses in global-scale convection models. To assess the effect of grid resolution on lid behavior we use 16 different resolutions keeping all physical parameters unchanged. To make sure that steady state has been reached each simulation is run for 15 Gyrs. Tested resolutions vary from 128x32 to 1024x256 grid points. To understand this influence on the tectonic regime we study the resolution within the lid requiring an appropriate lid definition, based on the thermal and velocity field. Our results show that there is a correspondence between low radial resolution and mobile lid regime and that low aspect ratio cells (azimuthal to radial grid spacing) favor a plate-like behavior of the lid, while for large aspect ratios the mobile lid regime is persistent.

This work is the first part of a larger project, aiming to study slab stagnation and hydration of the mantle transition zone (MTZ) using self-consistent global-scale mantle convection models, where subducting slabs carry water from the surface into the Earth's interior and potentially hydrate the MTZ. We expect that our previous work packages will help us to obtain realistic slab ponding in the MTZ, so we can study the hydration state of this region over time.

References

[1] Tackley, P. J. (2008). Modelling compressible mantle convection with large viscosity contrasts in a three-dimensional spherical shell using the yin-yang grid. *Phys. Earth Planet. Int.* 171, 7-18.

[2] Hernlund, J. W. and P. J. Tackley (2008). Modeling mantle convection in the spherical annulus. *Phys. Earth Planet. Int.* 171, 48-54.

P-14

The conditions of sublithospheric diamond formation constrained from ferric iron-rich exsolution from ferropericlase inclusions

C. MELAI[1], D. J. FROST[1], T. BOFFA BALLARAN[1], C. MCCAMMON[1]

[1] Bayerisches Geoinstitute , University of Bayreuth, Germany

Ferropericlase is apparently one of the more common inclusions to be found in sub-lithospheric diamonds, which are considered to form in the convecting mantle. Although relatively rare, these inclusions have been examined in a number of studies in the hope of providing information on the formation conditions of such deep diamonds, which could potentially be in the transition zone or lower mantle. The wide range of oxide Fe/(Fe+Mg) ratios found has raised the idea that they may form through the oxidation of iron metal. During TEM investigations, however, evidence for the exsolution of Fe_2O_3-rich phases such as magnesioferrite have been found, which implies that a more complex scenario may be involved. Ferropericlase-magnesiowüstite diamond inclusions are most likely some of the deepest available samples from the mantle and they potentially provide the most direct evidence for deep mantle carbon transport processes. The ferric iron contents of such inclusions alone may not provide a direct estimate for the oxygen fugacity at which the inclusions were trapped, particularly if pressure has a strong effect on the fO_2 - $Fe^{3+}/\Sigma Fe$ relationship. However, using experimental data it is possible to determine the oxygen fugacity at which the exsolution observed in the diamond inclusions occurred and coupled with the oxide $Fe^{3+}/\Sigma Fe$ ratio this could be used to estimate the pressure of formation.

The ferropericlase- magnesioferrite system has been investigated by several studies at room pressure but the stability field of the two components has been shown to become more complicated at high pressure due to the formation of mixed valence oxides. We have combined experimental measurements with thermodynamic modelling in order to address two main questions: at which P, T, fO_2 conditions do Fe_2O_3-rich phases exsolve from ferropericlase? And what is the maximum $Fe^{3+}/\Sigma Fe$ ratio of ferropericlase. To answer these questions, multianvil experiments have been performed between 6 – 25 GPa and 1200-1800°C using a starting composition of $(Mg_{86}Fe_{14})O$ plus 20 % Fe_2O_3. Pt powder was added to the experiments to act as a redox sensor and minor amounts of Ni, Cr, Mn and Na were also added. Samples were then analyzed with the scanning electron microscope, electron microprobe, Mössbauer spectroscopy and X-ray diffraction. In the recovered experiments ferropericlase coexists with magnetite-magnesioferrite solid solution up to 10 GPa and $Mg_2Fe_2O_5$-Fe_4O_5 solid solution at higher pressures. In the calculation of the oxygen fugacity a ferropericlase model in the FeO-$Fe_{2/3}O$-MgO system was employed and exchange of Mg and Fe^{2+} in magnetite was accounted for. Oxygen fugacities at which the phases coexist can be calculated in the magnetite-magnesioferrite field using three different equilibria and a quite simple ferropericlase mixing model results in calculated oxygen fugacities that are within 0.1 log units of each other for all three equilibria. The results show that magnetite-magnesioferrite solid solution should not be in equilibrium with ferropericlase in the diamond stability field. Our results imply that the exsolution of Fe^{3+} rich phases observed in natural samples likely occurred at pressures corresponding to the transition zone or deeper.

P-15

Shallow fluid circulation in mantle wedge inferred from the dihedral angle between olivine and NaCl-bearing aqueous fluid system

YONGSHENG HUANG[1], TAKAYUKI NAKATANI[1], MICHIHIKO NAKAMURA[1], CATHERINE MCCAMMON[2]

[1] Department of Earth Science, Graduate School of Science, Tohoku University, Aramaki-Aza-Aoba, Aoba-ku, Sendai, Miyagi 980-8578, Japan
[2] Bayerisches Geoinstitut, University of Bayreuth, 95440 Bayreuth, Germany

In subduction zones, the circulation slab-derived aqueous fluids are crucial to understand the origin of arc volcanism and further to constrain the global material recycling. The infiltration of aqueous fluids plays an important role on controlling geophysical properties of the mantle wedge such as elasticity, permeability and electrical conductivity. Recently, magnetotellulic studies found a high electrical conductor beneath the fore-arc which was interpreted as a storage of voluminous slab-derived fluid, implying the presence of permeable mantle wedge at fore-arc depths. By contrast, experimental constraints on dihedral(wetting) angle (θ) in the olivine-H_2O system indicated the fluid is once trapped in isolated pores (i.e., $\theta > 60°$) within the down-dragging mantle matrix at fore-arc depths and finally released just beneath the arc volcano where $\theta < 60°$. Here we present the precisely determined dihedral angles in the olivine and NaCl-bearing aqueous fluid (0–27.5wt% NaCl) system at 1–4 GPa and 800–1100°C to reveal the influence of NaCl, which is now recognized to be an important constituent of fluids in subduction zone, on the fluid connectivity. We found that NaCl significantly decreases θ down to below 60° at pressure and temperature conditions corresponding to the shallow mantle wedge even though the salinity even at 1 wt% NaCl. By combining our data with the results of geodynamic simulations, we infer that slab-released NaCl-bearing aqueous fluid starts to form an interconnected network in the mantle at relatively shallow depths (~80km) and can partly penetrate into the fore-arc crust without causing mantle melting. Our model also emphasized that partial melting of peridotite triggered by addition of aqueous fluid can occur more widely than previous perspective, suggesting that the transportation of aqueous fluid is not a primary control on the position of volcanic front.

This work was supported by the JSPS Japanese-German Graduate Externship.

P-16

Source estimation of ground tilt changes associated with small explosions at Stromboli volcano

AYUMU ISHIKAWA[1], TAKESHI NISHIMURA[1], HIROSHI AOYAMA[2], RYOHEI KAWAGUCHI[3], EISUKE FUJITA[4], TAKAHIRO MIWA[4], TAISHI YAMADA[4], MAURIZIO RIPEPE[5], RICCARDO GENCO[5]

[1] Department of Geophysics, Graduate School of Science, Tohoku University
[2] Graduate School of Science, Hokkaido University
[3] Meteorological Research Institute, JMA
[4] National Research Institute for Earth Science and Disaster Resilience
[5] Dipartimento di Scienze della Terra, Universita` di Firenze

Stromboli volcano is characterized by continuous activities of Strombolian explosions (small explosions) at summit craters. A lot of studies have investigated volcanic processes by multi-parameter observations. However, pressure source determination by geodetic measurements, which is indispensable to understand shallow magma reservoir which is a key for understanding magma dynamics, have not yet been well conducted because of insufficient geodetic observation network. In the present study, we analyze tilt records at 3 temporal and 2 permanent stations located closely to the summit craters to inverse the locations and size of pressure source by grid search analysis. Theoretical tilt vectors are calculated by using three-dimensional finite element method for considering the effect of topography.

5 tilt stations were installed at a distance of <1 km from the active craters of Stromboli. We analyze continuous tilt records of 5 stations during July 1 to July 15 when small explosion activity was high. We extract uplift and subsidence tilt signals associated with each of small explosion that are reported by Genco and Ripepe (2010) [1], and classify them in 4 stages: (A) Gradual uplift prior to small explosions, (B) Rapid uplift just before small explosions, (C) Rapid subsidence after small explosions, (D) Small uplift after (C). Tilt azimuths and amplitudes are almost same for the stages of (A) – (C), although LFS show about 30 degrees difference. We use the tilt vectors averaged for 680 events in the following analyses. We suppose that the pressure source is represented by an ellipsoidal cavity at beneath the summit craters. We searched optimal source model by grid search analysis. As a result, we find that the ellipsoidal cavity with a size of 200×100×400 m at 500 m depth beneath the summit craters represents 5% error. The pressure applied during the episode (A) is estimated to be about 10 kPa.

The size and position of the estimated ellipsoid is basically consistent with the picture of shallow magma reservoir inferred from an analysis of temporal evolution of flank lava effusion in 2007 (Ripepe et al., 2015) [2]. The mass and volume of magma supplied for conduit during a small explosion that are estimated from the obtained pressure change, appropriate conduit radius and magma density is comparable to the ejected mass and volume of one small explosion estimated from the observations of surface phenomena.

References

[1] Genco, R., and M. Ripepe (2010), Inflation‐deflation cycles reveal ed by tilt and seis mic records at Stromboli volcano,Geophys. Res. Lett., 37, L12302, doi:10.1029/2010GL042925.

[2] Ripepe, M., Delle Donne, D., Genco, R., Maggio, G., Pistolesi, M., Marchetti, E., ... & Poggi, P. (2015). Volcano seismicity and ground deformation unveil the gravity-driven magma discharge dynamics of a volcanic eruption. Nature communications, 6, 6998.

P-17

Single crystal elasticity of Fe-bearing phase E by Brillouin spectroscopy

NICCOLÒ SATTA[1], HAUKE MARQUARDT[2], ALEXANDER KURNOSOV[1], TIZIANA BOFFA-BALLARAN[1], JOHANNES BUCHEN[3], CATHERINE MCCAMMON[1], TAKAAKI KAWAZOE[4]

[1]Bayerisches Geoinstitut, University of Bayreuth, 95440 Bayreuth, Germany.
[2]Department of Earth Sciences, University of Oxford, South Parks Road, Oxford, UK.
[3]Seismological Laboratory, California Institute of Technology, Pasadena, California 91125, USA.
[4]Department of Earth and Planetary Systems Science, Hiroshima University, Hiroshima 739-8526, Japan.

Earth's deep water cycle plays a key role for dynamic evolution of our planet and the development of habitable conditions. Surface water can be transported to the Earth's mantle by subduction of oceanic lithosphere. Experimental investigations have shown that in cold subducting slabs, water can be efficiently stored in the Dense Hydrous Magnesium Silicates (DHMS). However, the quantification of the incoming water budget based on the interpretation of seismological observations is hampered by a lack of elasticity measurements of DHMS. Here, we report single-crystal elasticity measurements of phase E, a DHMS that is stable to pressure-temperature-conditions. A very low bulk modulus has been reported for phase E, suggesting that it might be able to produce seismic velocity heterogeneities detectable by seismological investigations. However, the shear modulus of phase E has never been quantified.

We synthesized Fe-bearing phase E single crystals in a multi-anvil apparatus. Chemical composition as well as crystal structure have been measured using electron microprobe, Mössbauer spectroscopy and single crystal X-ray diffraction. We determined the full elastic stiffness tensor by Brillouin spectroscopy employing two selected single crystals. At ambient conditions, we found phase E to have both the lowest bulk modulus and shear modulus among the DHMSs. Phase E shows very low compressional and shear velocities especially when compared to the other principal minerals likely present in subducting slabs. Modelling of seismic velocities in dry and hydrated upper mantle and transition zone rocks suggest that the presence of even small volume of phase E can appreciably lower seismic wave velocities. The elasticity of phase E under mantle conditions will be explored in future research.

P-18

Pargasite stability in the upper mantle at H_2O-undersaturated conditions

MARIJA PUTAK JURICEK[1], HANS KEPPLER[1]

[1] BGI, University of Bayreuth

Pargasitic amphibole is the most commonly occurring hydrous mineral in mantle xenoliths and investigation of pargasite stability at H_2O-undersaturated conditions can provide useful constraints for understanding deep water cycle.

While it has been shown that higher alkali content stabilizes pargasite to higher P and T, the effect of water on amphibole stability is not so straightforward. At H_2O-saturated conditions, alkali elements partition strongly into aqueous fluid and become less available for crystallization of amphibole. As a result, amphibole seemingly becomes stable at higher P and T when less H_2O is added to the starting material. This observation inspired the hypothesis that pargasite may be a ubiquitous phase in the upper mantle, which contains only a few hundred ppm of H_2O. However, previous studies determined pargasite stability at H_2O-saturated conditions, where solid phases coexist with an aqueous fluid during experiments. Such environments are not representative of the nearly dry ambient upper mantle.

Because of the high specific surface area of powders, adsorption of atmospheric H_2O on fine grained starting materials makes attaining defined H_2O activities by adding small amounts of water to the sample difficult or impossible. Instead, reduced water activities may be precisely controlled by diluting the water with another inert component. Under such conditions, solid phases are expected to coexist with a low water activity fluid throughout the experiment. As molecular nitrogen is mostly insoluble in upper mantle minerals, we used it in a series of piston cylinder experiments to buffer water activity of the fluid to a desired low value.

Our experiments demonstrate that pargasite is not stable in equilibrium with fluids diluted to X_{H2O}=0.1, while the amphibole stability field can extend to 4 GPa and above 1100 °C at high and intermediate water activities (X_{H2O}=1 to 0.5). This suggests that the ambient upper mantle has a nominally anhydrous assemblage while regions affected by metasomatic fluids may be more abundant in pargasite, and therefore retain more water, than previously thought.

P-19

Pb-isotope of Fe-Ni alloy associated with serpentinite: Geochemical constraints on the fluid-mediated hyper-reducing environment in mantle wedge

MAYU KAKEFUDA[1], TATSUKI TSUJIMORI[1,2], KATSUYUKI YAMASHITA[3], YOSHIYUKI IIZUKA[4]

[1] Department of Earth Science, Graduate School of Science, Tohoku University
[2] Center for Northeast Asian Studies, Tohoku University
[3] Graduate School of Natural Science and Technology, Okayama University
[4] Institute of Earth Sciences, Academia Sinica

Although the occurrence of Fe-Ni alloy is very limited in the vicinity of modern Earth's surface due to the highly oxidized state, serpentinization in the forearc mantle wedge can rarely provide extraordinary reducing environments that stabilizes the Fe-Ni alloy.

In order to understand those fluid-mediated hyper-reducing environments in serpentinizing mantle wedge of an active convergent plate margin, we revisited so-called 'josephinite' —an unusual 'metallic rock' composed mainly of Fe-Ni alloy (awaruite)— found in the Josephine Ophiolite, by engaging in microtextural and geochemical analyses.

Microtextural analyses using high-resolution FE-SEM and FE-EPMA found the presence of Ni-As mineral within aggregates of Fe-Ni alloy; the Ni-As mineral also occurs as discrete grains in 'josephinite'-hosting serpentinite, suggesting that Ni-As mineral acted as a precursor seed before the crystallization of Fe-Ni alloy.

Since each leachate obtained by stepwise leaching of a 'josephinite' pebble confirmed compositional homogeneity, this allows to calculate weighted mean values that give much precise Pb isotope compositions of aliquots of seventeen leaching steps determined by TIMS; the values yielded $^{207}Pb/^{204}Pb$ = 18.3378 ±0.0016, $^{206}Pb/^{204}Pb$ = 15.5693 ±0.0015, and $^{208}Pb/^{204}Pb$ = 38.0879 ± 0.0044. These newly obtained high precision Pb isotope compositions revealed that the 'josephinite'-forming fluids have a minor GLOSS-like sedimentary component. The presence of Ni-As mineral also supports the infiltration of arsenic-bearing external fluids derived from sedimentary rocks.

Considering the geological context of the Josephine Ophiolite, the 'josephinite'-forming fluids might have been derived from the top layer of subducting sediments. The lack of high-pressure metamorphic rocks such as blueschist in 'josephinite'-hosted serpentinite implies that the 'josephinite' formation might have occurred at a relatively shallow level of serpentinizing mantle wedge.

The absence of carbonate minerals further postulates that redox agent of the 'josephinite' forming hyper-reducing environment was H_2 evolved by the serpentinization rather than CH_4 that is commonly preserved in blueschist and eclogites. This fact would speculate a widespread hyper-reducing environment caused by H_2-rich fluids in a shallow level of serpentinizing mantle wedge.

Keywords: Fe-Ni alloy, serpentinization, Pb isotope composition, reducing fluid, mantle wedge

References

[1] Botto, R. I. and Morrison, G. H. (1976). Josephinite: a unique nickel-iron. *American Journal of Science*, v. 276, p. 241–274.
[2] Deschamps, F., Godard, M., Guillot, S., Chauvel, C., Andreani, M., Hattori, K., Wunder, B., France, L. (2012). Behavior of fluid-mobile elements in serpentines from abyssal to subduction environments: Examples from Cuba and Dominican Republic. *Chemical Geology*, v. 312–313, p. 93–117.
[3] Göpel, C., Manhès, G. and Allègre, C. J. (1990). U-Pb isotope systematics in josephinites and associated rocks. *Earth and Planetary Science Letters*, v. 97, p. 18–28.
[4] Hattori, K., Guillot, S. (2003). Volcanic fronts form as a consequence of serpentinite dehydration in the forearc mantle wedge. *Geology*, v. 31, p. 525-528.
[5] Sleep, N.H., Meibom, A., Fridriksson, T.H., Coleman, R.G., Bird, D.K. (2004). H2-rich fluids from serpentinization: Geochemical and biotic implications. *Proceedings of the National Academy of Sciences*, v. 101, p. 12818-12823.

P-20

Statistical correlation between tidal forces and swarm activity in the region of northern part of Wakayama Prefecture

KAZUKI MACHIDA[1], HIROYUKI NAGAHAMA[1], JUN MUTO[1]

[1] Department of Earth Science, Graduate School of Science, Tohoku University

Earthquakes occur when stress of the fault accumulates to the critical level. Smaller stress changes, such as the change of tidal forces, can trigger earthquakes in the critical state. For example, it is reported that before 2011 Tohoku Earthquake, the increase in the correlation between tides and earthquakes was reported [1]. Earthquakes with smaller magnitude are also prone to be affected by tides and expected to show tidal periodicities.

Previous research report that small earthquakes (e.g. in the northern part of Hyogo Prefecture) have correlation with Moon's age [2]. The exact periodicity of the earthquake cycle has not been revealed about these earthquakes. In recent research, correlation between tidal forces and earthquakes is analyzed by using statistical methods, such as Schuster test. The lower p-value of the Schuster test is, the more heterogeneous distribution in earthquakes versus phase of analyzed tides is. We analyzed shallow earthquakes in the northern part of Wakayama Prefecture from 1998 to 2016. This area is characterized by the presence of low-velocity anomaly beneath the swarm area implying that the seismic swarm is promoted by the presence of fluids [3].

The result of the Schuster test shows that the earthquakes in the region have low p-value around the period of Moon's age, 18-year cycle and tidal cycles of short periods (Fig. 1). Other research reported that this period is ascribed to change of barometric pressure [4]. The low p-value for the period T indicates that earthquakes have periodic variations at period T when sudden burst of earthquakes is excluded from data set [5]. The result suggests that earthquake cycle has the component of 18 days derived from variation of atmospheric pressure.

From the result of Schuster test, clear cycle that corresponds to Moon's age is not detected. We try to investigate the reason why heterogeneity in distribution for the period around 18 days appears.

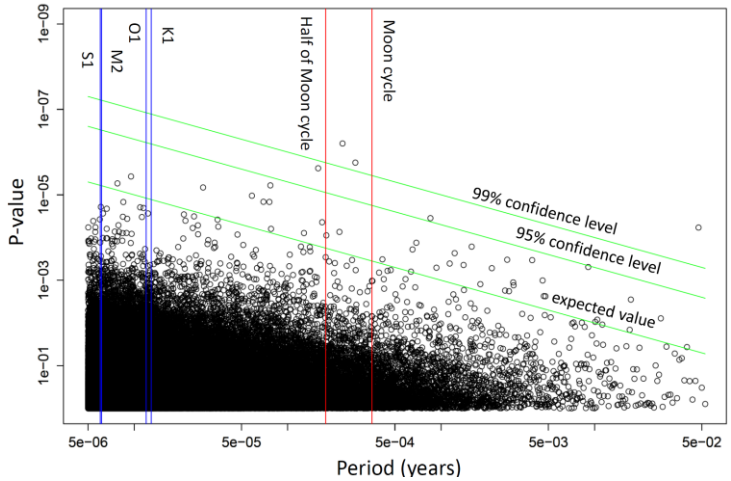

Fig. 1 Schuster spectrum of earthquakes. Blue and red lines indicate periods of tidal constituents and Moon's age. Red lines indicate expected value and confidence limits of p-value calculated from expected minimum p-value.

References

[1] Tanaka, S., 2012, Tidal triggering of earthquakes prior to the 2011 Tohoku-Oki earthquake (Mw 9.1), Geophysical Research Letter, 39, L00G26.
[2] Katao, H., 2002, Relation between Moon Phase and Occurrence of Micro-earthquakes in the Tamba Plateau, Journal of Geography, 111(2), 248-255.
[3] Kato, A., Saiga, A., Takeda, T., Iwasaki, T. and Matsuzawa, T., 2014, Non-volcanic seismic swarm and fluid transportation driven by subduction of the Philippine Sea slab beneath the Kii Peninsula, Japan, Earth, Planets and Space, 66, p86.
[4] Lauro, E. D., Petrosino, S., Ricco, C., Aquino, I. and Falanga, M., 2018, Medium and long period ground oscillatory pattern inferred by borehole tiltmetric data: New perspectives for the Campi Flegrei caldera crustal dynamics, Earth and Planetary Science Letters, 504, 21-29.
[5] Ader, T. J. and Avouac, J. -P., 2013, Detecting periodicities and declustering in earthquake catalogs using the Schuster spectrum, application to Himalayan seismicity, Earth and Planetary Science Letters, 377-378, 97-105.

P-21

Grain size dependency of olivine-spinel phase transformational mechanism responsible for deep-focus earthquakes

SANDO SAWA[1], JUN MUTO[1], NOBUYOSHI MIYAJIMA[2], HIROYUKI NAGAHAMA[1]

[1] Department of Earth Science, Graduate School of Science, Tohoku University
[2] Bayerisches Geoinstitut, University of Bayreuth

Deep-focus earthquakes occur at the depth from 440 km to 660 km in the subducting slab. The mechanism responsible for the earthquakes is thought to be different from that of shallow earthquakes, so that previous studies have reported the various mechanisms. By the geophysical observations and deformation experiments, the phase transformational faulting mechanism is presumed as the precursor of deep-focus earthquakes [1]. The phase transformational faulting mechanism is that metastable olivine in the slab undergoes the phase transformation to fine-grained spinel and faulting occurs with strain localization into the fine-grained spinel. This shear instability depends on grain size. Furthermore, the grain size may restrict the pressure- and temperature-condition where the shear instability occurs, that is, the region of slab where deep-focus earthquakes occur. However, previous studies have conducted deformation experiments with finer grain size than that in the slab [2]. Hence, the results from the laboratory experiments cannot directly apply to the geophysical observation. In this study, to reveal the grain size dependency on the phase transformational faulting, we conducted the deformation experiments of germanate olivine (about 3 μm), which is an analogue material of silicate olivine, finer-grained than that in previous studies (30 μm). We used a Griggs-type solid-confining media deformation apparatus. The confining pressure, temperature and strain rate are 1.2 GPa, 400~900 °C and 2.0×10^{-4}, respectively Even though deformation experiments were conducted under wider temperature conditions than previous studies, we did not observe any shear instability event with apparent stress drops. Also, Raman spectroscopy and electron back scattered diffraction pattern (EBSD) clarified that the germanate olivine underwent the transformation to spinel at temperatures higher than 500 °C. Despite a mixture of olivine and spinel at a temperature of 500 °C, shear instability does not occur because the difference in grain sizes between olivine and nucleated spinel in this study was smaller than those in previous studies. Also, the transformation temperature in this study was much lower than those in previous study (T > 1000 °C in [2]). Considering the rate equation of the transformation [3], small grain size promotes the transformation, but these fast rates of the transformation cannot be explained only by the effect of the grain size. Therefore, the presence of water such as absorbed water in a starting material can also contribute to promote the transformation. Hence, both small initial grain size and a little amount of water promote the transformation even at lower temperature. These results indicate that the phase transformational faulting mechanism has strong grain size dependency. In summary, the pressure- and temperature-condition where the faulting occurs depends on the grain size of olivine and amount of water. Because the grain size in the slab is larger than that in the experiments, by extrapolating from these results, we may restrict the region of slab where deep-focus earthquakes occur.

This work was supported by the JSPS Japanese-German Graduate Externship.

References

[1] Zhan et al. (2014), EPSL, vol 385, 89-96.
[2] Burnley et al. (1991), JGR, vol 96, 425-443.
[3] Chan (1956), Acta Metallurgica, vol 4, 449-459.

P-22

Incipient melting of nominally anhydrous minerals near hydrous solidus: an experimental study

NAOKO TAKAHASHI[1], TAKAYUKI NAKATANI[1], TATSUKI TSUJIMORI[1,2], MICHIHIKO NAKAMURA[1]

[1] Graduate School of Science, Tohoku University
[2] Center for Northeast Asian Studies, Tohoku University

Dehydration melting of nominally anhydrous minerals (NAMs) may occur in the regions that exceed the "storage capacity" of water such as the beneath ridges and the 410 km discontinuity in the Earth's interior [1]. However, direct experiments of the incipient melting of NAMs have not been confirmed due to difficulties in controlling low H_2O concentrations in system or analyzing small amounts of melt. In order to experimentally confirm the melting phenomena, we attempted piston-cylinder experiments using solid-solution end-member NAMs pairs (jadeite-spodumene: $NaAlSi_2O_6$-$LiAlSi_2O_6$) which have greatly different storage capacity of water. FT-IR measurements confirmed that the structural water content of natural jadeite (Jd) and spodumene (Spd) as starting materials were 90±27 ppm H_2O and up to 5 ppm H_2O, respectively. The single jadeite crystal (~1×1×2 mm) was placed in the spodumene powders (a few μm in diameter) without adding free water. A Pt-lined Ni capsule containing these pyroxenes were pressure-sealed at 2 GPa and then heated at 700°C for 36, 72, and 144 hours. Polished cross sections of the run products were observed with an optical mono-cathodoluminescence (CL) microscope and FE-SEM, and analyzed with EDS and WDS. At the surface of Jd crystal, we found the reaction zone with an intermediate composition (~$Jd_{24}Spd_{76}$-$Jd_{29}Spd_{71}$) was formed having a sharp interface with unreacted remnant Jd. Micron- to submicron-size polyhedral pores partially filled with silicate glass were observed in the reaction zones and reaction front. These features indicate that the mineral replacement has progressed via melt-mediated dissolution-precipitation rather than a diffusive solid-state Na-Li exchange. Previous studies in literatures postulate that our experimental conditions are below hydrous solidus of both jadeite and spodumene. Therefore, our experiments suggest that H_2O concentrations exceeding the storage capacity induced to lower melting temperature to near hydrous solidus and to produce incipient melt at Jd-Spd grain boundaries, which are regarded as an eutectic system. The existence of H_2O exceeding the storage capacity is likely explained by lower storage capacity of intermediate phase in the Jd-Spd solid-solution than that of Jd. Optical mono-CL microscopy revealed weak luminescence in the reaction zones, also suggesting that intermediate phase has low defect density related to hydroxyl. Our experimental results confirmed that even trace amount of water in excess of the storage capacity can lead to incipient melting of NAMs near hydrous solidus. Furthermore, the incipient melt may work as a solvent to enhance rapid mineral re-equilibrations via dissolution-precipitation in nominally anhydrous conditions.

References

[1] Hirschmann, M. M., Tenner, T., Aubaud, C., & Withers, A. C. (2009). Dehydration melting of nominally anhydrous mantle: The primacy of partitioning. *Physics of the Earth and Planetary Interiors*, *176*(1-2), 54-68.

P-23

Axisymmetric conductivities of Jupiter's middle- and low-latitude ionosphere

YUKI NAKAMURA[1], KOICHIRO TERADA[1], CHIHIRO TAO[2], NAOKI TERADA[1], YASUMASA KASABA[3], HAJIME KITA[4], AOI NAKAMIZO[2], AKIMASA YOSHIKAWA[5], SHINICHI OHTANI[6], FUMINORI TSUCHIYA[3], MASATO KAGITANI[3], TAKESHI SAKANOI[3], GO MURAKAMI[4], KAZUO YOSHIOKA[7], TOMOKI KIMURA[1], ATSUSHI YAMAZAKI[4], ICHIRO YOSHIKAWA[8]

[1] Department of Geophysics, Graduate School of Science, Tohoku University
[2] National Institute of Information and Communications Technology
[3] Planetary Plasma and Atmospheric Research Center, Tohoku University
[4] Institute of Space and Astronautical Science, Japan Aerospace Exploration Agency
[5] Department of Earth and Planetary Sciences, Kyushu University
[6] The Johns Hopkins University Applied Physics Laboratory
[7] Graduate School of frontier Science, The University of Tokyo
[8] The University of Tokyo

Ionospheric Hall and Pedersen conductivities are important parameters in determining the electric potential distribution and plasma convection in a magnetosphere-ionosphere system. At Jupiter, meteoric ions deposited by meteoroid ablation are expected to play a major role in the ionospheric conductivities (e.g., Cloutier et al., 1978 [1]). This study evaluates the contribution of meteoric ions to ionospheric conductivities and electric field in the inner magnetosphere.

We have developed a meteoroid ablation model, a photochemical model and an ionospheric potential solver. Our simulation results reveal that the largest contributions to the Hall and Pedersen conductivities occur in the meteoric ion layer because of the strong surface magnetic field at Jupiter. The conductance is axisymmetric in the middle and low latitudes because the lifetimes of meteoric ions in the lower ionosphere are sufficiently longer than half a Jovian day. At high latitudes, the conductance is enhanced at dawn side associated with the Region 2-like upward field-aligned current. The dawn-to-dusk electric field is 4 - 27 [mV/m] around Io's orbit. For comparison, we model another case of ionosphere without H+ and meteoric ions. In this case, the conductance is entirely smaller than the former case, and diminished at night side. The dawn-to-dusk electric field is 45 - 270 [mV/m] around Io's orbit.

In order to evaluate the validity of our results, we compare our results to observations. Previous studies showed that dawn-dusk brightness asymmetry in the Io plasma torus and dawnward shift of the position were caused by dawn-to-dusk electric field imposed on the inner magnetosphere (Ip and Goertz, 1983 [2], Barbosa and Kivelson, 1983 [3]). Observations by the Hisaki satellite revealed the existence of dawn-to-dusk electric field of ~4 - 9 [mV/m] around Io's orbit (Murakami et al., 2016 [4]). Our model results are almost consistent with the Hisaki observations in the case with meteoric ions in the lower ionosphere.

References

[1] Cloutier, P. A., R. E. Daniell, A. J. Dessler, and T. W. Hill, (1978), A cometary ionosphere model for Io, *Astrophysics and Space Science*, vol. 55, no. 1, p.93-112.
[2] Ip, W. -H., and C. K. Goertz, (1983), An interpretation of the dawn-dusk asymmetry of UV emission from the Io plasma torus, *Nature*, vol. 302, p. 232, 233.
[3] Barbosa, D. D., and M. G. Kivelson, (1983), Dawn-dusk electric field asymmetry of the Io plasma torus, *Geophysical Research Letters*, vol. 10, p. 210-213.
[4] Murakami, G., K. Yoshioka, A. Yamazaki, F. Tsuchiya, T. Kimura, C. Tao, H. Kita, M. Kagitani, T. Sakanoi, K. Uemizu, Y. Kasaba, I. Yoshikawa, M. Fujimoto, (2016), Response of Jupiter's inner magnetosphere to the solar wind derived from extreme ultraviolet monitoring of the Io plasma torus, *Geophysical Research Letters*, Volume 43, Issue 24, pp. 12,308-12,316

P-24

Source location of volcanic earthquakes and tremors at Sakurajima volcano based on seismic correlation

THEODORUS PERMANA[1], TAKESHI NISHIMURA[1], HISASHI NAKAHARA[1]

[1] Department of Geophysics, Graduate School of Science, Tohoku University

Precise source locations of volcanic tremors and earthquakes are one of the most basic information important to understand the volcanic process. The spatio-temporal changes of these source locations may provide insight into the eruption mechanism and the movement of volcanic fluids. However, the determination of those source locations is quite challenging due to the difficulties to distinguish their seismic phases and precisely measure the arrival times. Recently, we developed a hypocenter determination method for volcanic earthquakes and tremor, which adopts seismic interferometry processing technique [1] for calculating cross-correlation functions (CCFs) and the source-scanning algorithm (SSA) [2] as proposed by [3]. Here, we apply our method to observed data recorded at Sakurajima volcano. We first locate volcano-tectonic earthquakes (VTs) and evaluate the errors by comparing the results with the hypocenters determined by a phase-picking method. Then, we locate volcanic tremors and discuss their source locations, which cannot be obtained from phase-picking methods due to indistinguishable phase arrivals.

We analyze VTs that occurred during a rapid dike intrusion on August 15, 2015. Our result shows the hypocenters are distributed beneath the Mt. Minamidake mainly at 0-4 km depths. Our source locations are consistent with the hypocenters obtained by using a conventional phase-picking method [4] and the errors are estimated to be 2 km or less.

We determine the source locations of two kinds of tremors occurring on August 22-25, 2017. One is 13.5 hours long continuous tremor accompanying strombolian eruptions on August 22-23. Another one is a series of intermittent tremors are recorded following the explosion earthquakes associated with Vulcanian eruptions that followed the continuous tremor. We calculate CCFs at 1-3 Hz by using 20 s time windows with 19 s overlap for these tremors and stacked them to obtain average CCFs. Our results show that the source locations of the first 6 hours of continuous tremor, which are determined every 10 minutes, are located beneath Mt. Minamidake at depths from about 3 km to the active crater. The sources of the following continuous tremor are located at shallower depths, about 2 km depth to the ground surface on the southern flank of Mt. Minamidake. The sources of 61 segments of the intermittent tremors are densely distributed at 0-2 km depth beneath Mt. Minamidake.

The observed tremors are related to the eruptive activities at Sakurajima volcano and their sources are expected to be located at the eruptive conduit. Our estimated sources are distributed at the shallow depths beneath the active craters within the estimated errors. Therefore, our results show the prospect of our method as an alternative for tremor source location determination and volcano monitoring. The depth range of our results for continuous tremor also coincides with the previous studies on the generation depth of volcanic earthquakes [5].

References

[1] Bensen *et al*., 2007. Location of tremor sources and estimation of lava output using tremor source amplitude on the Piton de la Fournaise volcano: 1. Location of tremor sources, *J. Volcanol. Geoth. Res.*, 147(3-4).

[2] Droznin *et al*., 2015. Detecting and locating volcanic tremors on the Klyuchevskoy group of volcanoes (Kamchatka) based on correlations of continuous seismic records, *Geophys. J. Int*., 203(2)

[3] Permana *et al.,* _. Reliability evaluation of volcanic tremor source location determination using cross-correlation functions, submitted.

[4] Hirata & Matsuura, 1987. Maximum-likelihood estimation of hypocenter with origin time eliminated using nonlinear inversion technique, *Phys. Earth Planet. Inter*., 47

[5] Iguchi, M., 1994. A vertical expansion source model for the mechanisms of earthquakes originated in the magma conduit of an andesitic volcano: Sakurajima, Japan. *Bull. Volcanol. Soc. Japan*, 39.

P-25

Experimental constraints on the composition of subduction zone fluids

GRETA RUSTIONI[1], ANDREAS AUDÉTAT[1], HANS KEPPLER[1]

[1] Bayerisches Geoinstitut, Universität Bayreuth, 95440 Bayreuth, Germany

The nature of the slab-derived mobile phase that metasomatizes the mantle wedge and causes melting in volcanic arcs is still poorly understood. Recent models argue that a transport mediated by aqueous fluids is too inefficient to produce the observed trace element enrichment in arc magmas. Instead, sediment melts were proposed as the main metasomatizing agents [1-5].

In a series of piston cylinder experiments conducted at 4 GPa and 700-800 ˚C, we studied the effect of NaCl on the partitioning of trace elements between aqueous fluids and an eclogitic residue. The investigated fluid compositions ranged from pure water to 15 wt. % NaCl, covering the most common fluid salinities in subduction zones. In our experiments, fluid/eclogite partition coefficients for a set of 25 trace elements were determined by laser-ablation ICP-MS analyses using the diamond trap technique. The good agreement between forward and reversed experiments (in which all the trace elements were doped into the fluid phase instead of the solid starting material) demonstrates the attainment of equilibrium.

The results show that the partitioning of the light rare earths, alkalis, alkaline earths, Pb, and U into the fluid is enhanced by several orders of magnitude upon addition of a few wt. % of Cl. For some of these trace elements, the solubility increase is comparable to that for a temperature increase by several hundred ˚C. On the other hand, the partitioning of the heavy rare earths and high field strength elements seem to not be affected by fluid salinity, thus enhancing features typically observed in arc magmas such as the negative Nb-Ta anomaly.

Overall, our data indicate that the trace element enrichment observed in typical arc magmas is entirely consistent with hydrous fluids being the main trigger for melting in subduction zones. Sediment melting is likely a phenomenon of only local importance for arc magmatism.

References

[1] Kelemen, Hanghøj & Greene (2005), Treatise of Geochemistry, The Crust, vol. 3, p. 593-659.
[2] Hermann, Spandler, Hack & Korsakov (2006), Lithos 92, 399-417.
[3] Skora & Blundy (2010) Journal of Petrology 51, 2211-2243.
[4] Behn, Kelemen, Hirth, Hacker & Massonne (2011), Nature Geoscience 4, 641-646.
[5] Spandler & Pirard (2013), Lithos 170-171, 208-223.

P-26

Moment tensor inversion of very-long-period seismicity using very-near-field seismic records at Stromboli volcano

SHUNSUKE SUGIMURA[1], MAURIZIO RIPEPE[2], GIORGIO LACANNA[2], DENIS LEGRAND[3], SÉVASTIEN VALADE[4]
TAKESHI NISHIMURA[1]

[1] Department of Geophysics, Graduate School of Science, Tohoku University
[2] Department of Earth Sciences, University of Florence, Italy
[3] UNAM University, Mexico
[4] GFZ-German Research Centre for Geosciences, Potsdam, Germany

In the last decades, moment tensor inversion of very-long-period (VLP, 2-100 s) earthquakes associated with volcanic activity has been applied to estimate the optimal source location and mechanism. Based on this analysis, VLP associated with explosions at Stromboli volcano have been interpreted as the pressure source of opening/closing cracks embedded in the volcanic medium (Chouet et al., 2003 [1]) and located outside the crater rim along the Sciara del Fuoco slope. We present the analysis of data collected in September 2016 by eight broadband seismic stations deployed in the very-near-field condition, at only 100-300 m away from the active craters.

We apply the moment tensor inversion to VLP (0.05-0.2 Hz) signals associated with infrasonic signals located by the array at the north-east (NE) crater. However, the result of the inversion shows that the optimal centroid, above the 95% of confidence, is located at 200 m southwest of and 160 m beneath the NE crater. We found that the source mechanism is greatly dominated by the vertical component of the moment tensor, with inverted polarity of the two other isotropic components result inverted. The squared error between the observed and synthetic waves (Ohminato et al. 1998 [2]) is only 11%.

However, the squared errors are widely distributed covering a volume 150 m x 100 m large in the horizontal around the NE crater and 350 m deep in the vertical direction. If we force the source to be located just below the NE crater and at a depth of 160 m, the error becomes of only 18 % and the solution still remains within the 95% confidence interval. For this new location, the source mechanism becomes dominated by three isotropic components with a same polarity.

A model resolution matrix based on the Green's functions indicates that the three isotropic components have resolution lower than the deviatoric ones suggesting that the isotropic components of the source mechanisms are not very well constrained even by using very-near-field seismic network. We believe that this instability of the moment tensor inversion is opening discussion on the meaning of the volumetric change in the conduit or magma chamber inferred by seismic signal.

Keywords: moment tensor inversion, source mechanism, VLP, Stromboli volcano, very-near-field, model resolution matrix

References

[1] Chouet, B., P. Dawson, T. Ohminato, M. Martini, G. Saccorotti, F. Giudicepietro, G. De Luca, G. Milana, and R. Scarpa (2003), Source mechanisms of explosions at Stromboli volcano, Italy, determined from moment-tensor inversions of very-long-period data, J. Geophys. Res., 108(B1), 2019, doi:10.1029/2002JB001919.

[2] Ohminato, T., B. A. Chouet, P. B. Dawson, and S. Kedar (1998), Waveform inversion of very-long-period impulsive signals associated with magmatic injection beneath Kilauea volcano, Hawaii, J. Geophys. Res., 103, 23,839–23,862.

Earth, Sea, and Sky V:
International Joint Graduate Program Workshop in Earth and Environmental Sciences
co-hosted by The International Joint Graduate Program in Earth and Environmental Sciences, Tohoku University (GP-EES)
and JSPS-DFG Japanese-German Graduate Externship for Research on Deep Earth Volatile Cycle
June 2-4, 2019. Aobayama Campus, Tohoku University

P-27

Spatial distribution of S wave reflectors beneath the Yonezawa-Kitakata region, northeastern Japan

MANAMI SUZUKI[1], TOMOMI OKADA[1], AKIKO HASEMI[2], GROUP FOR THE AFTERSHOCK OBSERVATIONS OF THE 2011 OFF THE PACIFIC OF TOHOKU EARTHQUAKE

[1] Department of Geophysics, Graduate School of Science, Tohoku University
[2] Department of Earth Science, Graduate School of Science, Yamagata University

One of the factors of volcanic activity and seismic activity in the Tohoku district is fluids present in the crust. This fluid is considered to form seismic wave low velocity region or seismic reflection beneath volcanic area and active fault. (e.g., Hori et al., 2004 [1]) The Yonezawa-Kitakata region in the southern part of the Tohoku region was located in the west of Nishiazuma Volcano and Bandai Volcano. In the Yonezawa-Kitakata area shallow microearthquake swarm started at 7 days after the 2011 off the Pacific coast of Tohoku Earthquake where the seismic activity was low before the Tohoku-Oki earthquake. some previous studies suggest that the cause of the triggered seismicity occurred due to increase of fluid pressure. (e.g., Okada et al., 2015 [2]). The objective of this study is to estimate the areas of fluid by investigating distribution of S wave reflectors, consider the relevance to inland earthquake occurrence.

We use temporary seismic network deployed by Kochi University, Chiba University, and Tohoku University, to investigate more detailed distribution of reflectors in addition to the Hi-net stations. We used waveforms observed at these stations from 4798 events in the period from May 2011 to February 2012. We used hypocenter locations obtained by the double-difference method (Waldhauser and Ellsworth, 2000 [3]). We applied the automatic amplitude control (AAC) correction and 4-16 Hz band pass filler to these waveform data, and we made some seismograms along various profiles for each station. Next, in order to estimate the depth of the S wave reflectors, we also made some seismograms by converting time to depth (Inamori et al., 1992 [4]). We picked reflected wave from the stations that show clear reflected waves using seismograms we made, obtained the image station where the difference from the calculated arrival time (t_{cal}) and observed arrival time (t_{obs}) was smallest (Horiuchi et al., 1997 [5]). Furthermore, we calculated the striking and dipping of the reflectors and the location of the reflected point by each hypocenter. The velocity structure was uniformly assumed to be 3.4 km/s.

As a result, the reflectors are located from the lower part of the source region to the depth of 10 - 20 km below it. The strike seems to be drawing a circle or an arc, and the dips are smaller beneath the source region. Comparing this reflector distribution with the seamless geological map [AIST], for the reflectors just beneath the Otoge caldera their strikes seems to be along the edge of the caldera, and for the reflector in the western part, their strikes follows the western marginal fault zone of Aizu Basin and the boundaries of geological structure. Comparing this with the seismic velocity structure, the reflectors are located at the periphery of the low velocity zone, being consistent with the results obtained by previous study. By this reason, fluids promoting swarm earthquakes in the Yonezawa - Kitakata area may be migrated from the melt below the epicenter area and may have passed boundary of the existing geological structure.

The seismic waveforms were aligned so as to follow the surveyed lines (we call this “recorded cross section (RCS) ”) in the north-south/east-west directions. In each RCS, if three or more phases are aligned at about 1.5 times or more than the ambient amplitude at the same depth, it is defined to be a reflected wave, and arrival depths of initial motion were read. When a reflected wave was detected at the same depth at the intersection of RCS, we interpreted that it was reflected from the same reflection surface. When multiple reflected waves can be confirmed in one RCS, we read multiple waves, respectively. As a result, 16 reflectors in the northeast clusters, 14 in the center, and 3 in the southwest were read.

References

[1] Hori. S., N. Umino., T. Kono., A. Hasegawa., (2004), Distinct S-wave Reflectors (Bright Spots) Extemsively Distributed in the Crust and Upper Mantle beneath the Northeastern Japan Arc, J. Seismol. Soc. Jpn., Ser. 2 (56), 435-446 (in Japanese).

[2] Okada. T., T. Matsuzawa., N. Umino., K. Yoshida., A. Hasegawa., H. Takahashi., T. Yamada., M. Kosuga., T. Takeda., A. Kato., T. Igarashi., K. Obara., S. Sakai., A. Saiga., T. Iidaka., T. Iwasaki., N. Hirata., N. Tsumura., Y. Yamanaka., T. Terakawa., H. Nakamichi., T. Okuda., S. Horikawa., H. Katao., T. Miura., A. Kubo., T. Matsushima., K. Goto and H. Miyamachi. (2015), Hypocenter migration and crustal seismic velocity distribution observed for the inland earthquake swarms induced by the 2011 Tohoku-Oki earthquake in NE Japan: Implications for crustal fluid distribution and crustal permeability. Geofluids, 15(1-2), 293–309. https://doi.org/10.1111/gfl.12112

[3] Waldhauser. F., Ellsworth. B., (2000), A double-difference earthquake location algorithm: method and application to the Northern Hayward Fault, California. Bulletin of the Seismological Society of America, 90, 1353–1568.

[4] Inamori, T., S. Horiuchi and A. Hasegawa., (1992), Location of mid-crustal reflectors by a reflection method using aftershock waveform data in the focal area of the 1984 Western Nagano Prefecture earthquake, J. Phys. Earth, 40, 379-393.

[5] Horiuchi, S., N. Tsumura and A. Hasegawa, (1997), Mapping of a magma reservoir beneath Nikko-Shirane volcano in northern Kanto, Japan, from travel time and seismogram shape anomalies, J. Geophys. Res., 102, 18071-18090.

P-28

Constraint for the formation temperature of the dark inclusion in a CK chondrite by thermodynamic equilibrium calculation

MIKI TAKAHASHI[1], TOMOKI NAKAMURA[1], TAKAZO SHIBUYA[2], MICHAEL E. ZOLENSKY[3]

[1] Department of Earth Science, Graduate School of Science, Tohoku University
[2] Japan Agency for Marine‐Earth Science and Technology (JAMSTEC).
[3] Astromaterials Research and Exploration Science, NASA Johnson Space Center.

■Introduction

Dark inclusions are dark fragments in sub-mm to centimeter in size found in many meteorites. They accreted onto the meteorite parent asteroids that are much smaller than the earth, therefore they escaped high-speed impact upon accretion and thus survived even if they are fragile material. Many meteorites flying directly to the earth are thought to have come from some resonance orbits Kirkwood gaps in the inner asteroid belt, but small rock fragments flying to asteroids are come from outer asteroids and comets. We performed mineralogical study of a dark inclusion in the NWA 2900 CK3.5-3.7 carbonaceous chondrite and found many large veins of diopside in the dark inclusion [1]. Such veins have never been found from any carbonaceous chondrites. In this study, we constrained thermodynamically the temperature at which the dark inclusion was formed, based on the mineralogical chemistry and the bulk chemical composition of the dark inclusion.

■Petrology and mineralogy

The dark inclusion is 1.0×2.5 cm size and consists mainly of dark and fine-grained material (typically <20μm but occasionally 100μm in grain size). It does not contain chondrules, but contains many bright veins. The fine-grained material consists mainly of olivine ($Fa_{34.8\pm0.52}$), magnetite, plagioclase ($Ab_{63.6\pm7.1}$, $An_{35.8\pm7.3}$), Cr spinel, and a small amount of tiny pentlandite. On the other hand, the bright veins (~1cm long and ~100μm width) go through an entire region of the dark inclusion and connects with other veins, forming a network structure. Besides the long veins, many small veinlets (~100μm long) also occur. The veins and veinlets consist mainly of crystalline diopside with high Wo contents (Wo>40), some variations of Mg/(Mg+Fe+Ca) ratio (51.9>En>31.1), and low concentrations of minor elements such as Al, Na, Mn, Cr, and Ti. The relative abundance of the major five minerals, normalized to 100wt%, in the dark inclusion is estimated to be olivine 61.8wt%, diopside 16.8wt% magnetite 14.8wt%, plagioclase 4.0wt%, and spinel 2.6wt%.

■Method of thermodynamic calculation

1. The bulk composition of the dark inclusion (about 6×18mm) was obtained by FE-EPMA analysis.
2. Thermodynamic equilibrium state with coexisting bulk rock and water was calculated (physical conditions: water/rock ratio= 0.25, 1, 2.6, and 4; initial water pH=7; the pressure=5kbar at 400-1000°C).
3. Five major minerals in the dark inclusion were analyzed by FE-EPMA to determine chemical composition of individual minerals.
4. The relative mineral abundance was estimated from major-elemental abundance in each mineral and that of whole dark inclusion.
5. The obtained relative mineral abundance and chemical composition of the constituent minerals were compared with those estimated by thermodynamic equilibrium calculation.

■Discussion

The diopside compositional features such as high Wo and En contents and low minor-element concentrations and the absence of phyllosilicate in the inclusion are consistent with high-temperature hydrothermal origin of the dark inclusion and the diopside veins [e.g., 2-3]. The results of thermodynamic calculation indicate that the dark inclusion formed at temperature higher than 800°C. No carbonaceous chondrites have experienced aqueous alteration at such a high temperature. Assuming that heat source is ^{26}Al heating, the dark-inclusion is likely to have formed before chondrule formation. The timing of formation depends on the water/rock ratios (water-rich asteroids are difficult to be heated and thus are required to form earlier). Because water-free asteroids need to be formed at 2.2 Myr after CAIs to reach the peak temperature of 800°C [4], the dark inclusion must have formed before this. The early timing of formation is consistent with the observation that chondrules are absent in the dark inclusion and that host CK chondrite is an accretionary breccia.

References

[1] Takahashi et al. 2019. 82th Meteoritical Society Meeting, submitted.
[2] Bird et al. 1984. *Economic Geology* 79:671-965.
[3] Robinson et al. 2002. *Proceedings of the Ocean Drilling Program, Scientific Results* 176.
[4] Wakita et al. 2014. *Meteoritics & Planetary Science* 49:228-236.

P-29

Intra-seasonal variability of oceanic low-level cloud in summertime North Pacific and its interaction with sea surface temperature

NAOYA TAKAHASHI[1], TADAHIRO HAYASAKA[1]

[1] Center for Atmospheric and Oceanic Studies, Department of Geophysics, Graduate School of Science, Tohoku University

Oceanic low-level cloud plays a key role to determine radiation budget at the surface or top-of-atmosphere and modulate regional and global climate variabilities [1]. In particular, an interaction between oceanic low-level cloud and sea surface temperature (SST) is important process to understand co-variability of atmosphere, sea surface, and subsurface layer [2]. Despite the importance of role of the low-level cloud, the detailed process of evolution of the cloud and the air-sea interaction associated with low-level cloud variability is not well investigated on shorter time-scale than seasonal variation.

In the present study, we investigated the intra-seasonal variability (ISV) of oceanic low-level cloud cover (LCC) and associated interaction process with ocean in the western north Pacific by using satellite observational and reanalysis datasets from 2003 to 2016. Typical time-scales of LCC variability in the North Pacific are synoptic scale (3-7-day) and intra-seasonal scale (20-100-day), which is shorter than seasonal variation. Important LCC controlling factors are SST and horizontal temperature advection (Tadv), whose dominant time-scales of are similar with that of LCC. We focused on ISV of LCC, SST and Tadv in this study because coherence among each variable on intra-seasonal time-scale is higher than synoptic one. From band-pass filtering method and phase composite analysis for investigating the evolution process of LCC anomaly, it is found that ISV of LCC is almost stationary. It implies that local cloud-controlling factor is important to evolution of low-level cloud. The results also showed that horizontal dry-cold advection from poleward is a trigger to increasing in LCC but SST is follower by LCC due to cloud radiative effect for shortwave radiation (Fig. 1). Evolution of LCC is also corresponded to positive tendency of RH (not shown). Positive tendency of RH is generated by change in not specific humidity but temperature (i.e. decreasing saturation water vapor due to decreasing temperature). We further quantitatively investigated the impact of LCC to SST by oceanic mixed-layer temperature budget analysis, showing that an importance of anomalous dry-cold advection to cooling of SST by not only enhanced latent heat release but also decreasing in downward shortwave radiation at the sea surface by more low-level cloud cover. An active role of SST to LCC is not clearly confirmed in this study (Fig. 2), however, a sensitivity test using numerical simulation is one of effective methods to investigate the active impact of SST to low-level cloud in the mid-latitude.

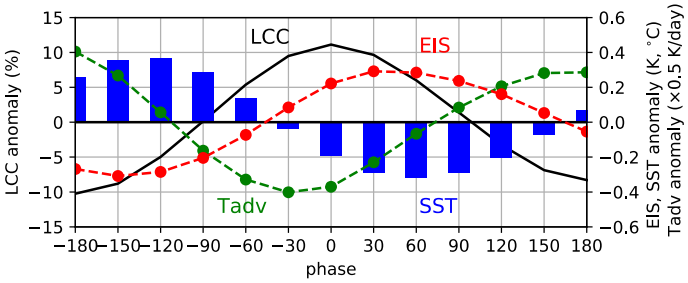

Fig. 1
Evolution of composited anomalies of LCC (black), SST (blue), Tadv (green), and EIS (red) which are averaged in the target area (165-175 ˚E, 30-40 ˚N). X-axis show 13 phases determined by phase composite analysis method based on variation of area-mean filtered LCC anomaly.

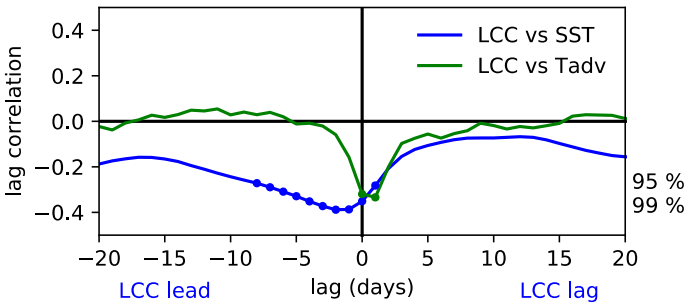

Fig.2
Lag correlation coefficient between LCC and SST (blue), LCC and Tadv (green) derived from unfiltered daily datasets. Horizontal dashed (solid) line indicates minimum correlation coefficient exceed with 95 (99) % significance level.

References

[1] Hartmann and Short 1980, *Journal of the Atmospheric Sciences*, **37**, 1233-1250
[2] Wang et al. 2012, *Journal of Climate*, **25**, 1619-1634, DOI:10.1175/JCLI-D-11-00704.1

P-30

Variation of coseismic fault displacements on multiple seismic cycles at a site: An example from the Kamishiro fault, Itoigawa-Shizuoka Tectonic Line active fault system, central Japan

NAOYA TAKAHASHI[1], SHINJI TODA[2]

[1] Department of Earth Science, Graduate School of Science, Tohoku University
[2] International Research Institute of Disaster Science, Tohoku University

Predicting coseismic fault slip at a site on an active fault is crucial from the view point of fault displacement hazard assessment. The characteristic earthquake model, where an amount of coseismic slip at a point on a fault is roughly consistent through seismic cycles [1], has been widely accepted and applied for hazard assessment. However, recent paleoseismic studies, high-resolution topographic data and quantitative more precise dating techniques have revealed that many faults do not repeat persistently their characteristic displacements [2]. To further discuss this issue, however, more case studies in particular on a dip-slip fault are required.

We estimated co-seismic slips of paleo-earthquakes at Oide site (36.7°N, 137.87°E) on the Kamishiro fault and evaluated variability in co-seismic slips through seismic cycles. The Kamishiro fault is a reverse fault which is located at the northernmost part of the Itoigawa-Shizuoka Tectonic Line active fault system in Japan. Advantages of this fault are that the co-seismic slip distribution of the most recent event, the 2014 Nagano-ken-hokubu earthquake (Mw 6.2), is precisely measured by field observation and differential LiDAR analysis, and that there is a flight of displaced terraces that record slips of recent earthquakes. Several paleoseismic studies share the evidence for the penultimate and the antepenultimate events that occurred in AD 1714 and ~1.2 ka (AD 841 or AD 762) respectively, whereas the event ages older than 1.2 ka are not well constrained. Here we mapped five displaced terraces (T1-T5, from the older) at Oide using aerial photographs taken by the US Armed Forces in the 1940s. Then, we estimated cumulative net slip of T1, T2 and T5 terraces using a tool developed by [3] which incorporates topographic and fault properties with uncertainties and enables us to objectively estimate a plausible cumulative net slip. We made 30 topographic profiles for each terrace, and sought the mean and standard deviation of the cumulative net slip. We also constrained terrace ages based on radio carbon dating. As a result, we estimated coseismic slips of the penultimate and the antepenultimate events, 1.5±0.2 m and 2.7±0.4 m, respectively. Next, we performed a Monte Carlo simulation to estimate slips of events before the antepenultimate earthquake and then explore a possible range of CV (Coefficient of Variation) for co-seismic slips. CV is a ratio of a data set's standard deviation to mean and used to assess variability. Low CV indicates co-seismic slips are nearly the among seismic cycles, and high CV (close to 1) means slips are variable. Because previous paleoseismic studies found one to three earthquakes occurred between T1 formation (5-2.7 ka) and 1.2 ka, we iteratively computed one to three co-seismic slips before 1.2 ka so that the simulated slip sequences can reproduce the cumulative terrace offsets. This approach enabled us to calculate CV that ranged from 0.3 to 0.5 (1σ), which indicates that a recent sequence of co-seismic slips at Oide does not follow the characteristic earthquake model but varies in a narrow range.

References

[1] Schwartz D. P. and Coppersmith K. J., (1984), Journal of Geophysical Research, 89, B7,5681-5698.
[2] Zielke O., (2018), Bulletin of Seismological Society of America, 108, 3A, 1399-1413.
[3] Wolfe F. D. et al., (2018), American Geophysical Union fall meeting, S41D-0575.

Earth, Sea, and Sky V:
International Joint Graduate Program Workshop in Earth and Environmental Sciences
co-hosted by The International Joint Graduate Program in Earth and Environmental Sciences, Tohoku University (GP-EES)
and JSPS-DFG Japanese-German Graduate Externship for Research on Deep Earth Volatile Cycle
June 2-4, 2019. Aobayama Campus, Tohoku University

P-31

Normal stress dependency of E_1' center in simulated quartz gouge by brittle fracture

KIRIHA TANAKA[1], JUN MUTO[1], YASUO YABE[2], TOSHITAKA OKA[3], HIROYUKI NAGAHAMA[1]

[1] Department of Earth Science, Graduate School of Science, Tohoku University
[2] Department of Geophysics, Graduate School of Science, Tohoku University
[3] Department of Chemistry, Graduate School of Science, Tohoku University

Fault dating method by electron spin resonance (ESR) is determining an age of the last fault movement or fault formation. This method is based on a hypothesis that unpaired electrons trapped in defects in quartz are accumulated by natural radiation and annealed by a fault movement [1]. This hypothesis has not been understood completely [2]. Ikeya et al. [1] performed compression tests for quartz grains in a stainless vessel and E_1' center decreased with increasing normal stress and Tanaka [3] sheared silica sands between stainless cylinders using a rotary shear apparatus and E_1' center decreased with increasing normal stress. However, Hataya and Tanaka [4] have found that stainless affects ESR spectra. Therefore, we performed shear tests with brass cylinders at different normal stresses using a low-velocity rotary shear apparatus and ESR measurements.

We used silica sands bought from the Association of Powder Process Industry and Engineering (APPIE), Japan, as starting quartz gouges. The silica sand is 45-300 μm in diameter and consists of 95 % SiO_2 with a small amount of impurities. Shear tests were conducted for the gouge with a displacement of 0.56 m, slip rate of 0.76 mm/s and normal stress up to 15.4 MPa. ESR measurement for E_1' center were performed for starting and sheared gouges at room temperature, microwave power of 0.01 mW (ESR-1). To confirm the effect of contaminants on ESR intensity, the same ESR measurements were also performed for starting gouge and those mixed with contaminants (ESR-2).

ESR intensity increased with normal stress up to 2.9 MPa and decreased with further increases in normal stress from 4.9 to 15.4 MPa (Figure 1). Effect of heating on ESR intensity is negligible because maximum temperature rise at grain contacts is estimated to be about 140 K [5] which is smaller than inflection temperature of ESR intensity for E_1' center. Effect of contaminants on ESR intensity is negligible due to the results of ESR-2. SEM observations clarified the significant grain size reduction of gouges after tests. Therefore, the effects of stress concentration or brittle fractures seem to be attributed to the ESR intensity change. We consider two possible interpretations of this ESR intensity change. Firstly, the ESR intensity for E_1' center depends on grain size reduction by brittle fracture and it stops at normal stress of 2.9 MPa. Secondly, E_1' center is produced and annealed by grain size reduction and stress concentration, respectively.

From these results, ESR intensity is likely to be zeroed by rock deformation or fracture normal stress larger than 60 MPa. This indicates that fault dating method by ESR may be applicable for deeper faults. In addition, this result also implies that E_1' center may become an index reflecting on a transition point of grain size reduction or stress concentration by fault motions.

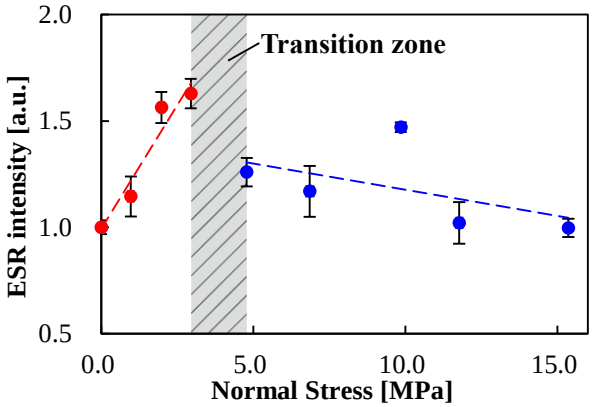

Figure 1. The relationship between ESR intensity for E_1' center and normal stress. Dotted lines indicate linear approximation curves of red and blue dots.

References

[1] Ikeya, M., Miki, T., Tanaka, K., 1982. Dating of a fault by electron spin resonance on intra-fault materials. *Science*, 215, 1392-1393.
[2] Yang, H.L., Chen, J., Yao, L., Liu, C.R., Shimamoto, T., Thompson J.J.A., 2019. Resetting of OSL/TL/ESR signals by frictional heating in experimentally sheared quartz gouge at seismic slip rates. *Quaternary Geochronology*, 49, 52–56.
[3] Tanaka, K. 1987. Investigations on the ages of fault movements by electron spin resonance (ESR) dating method - Experiments on the zero-setting of the paramagnetic defects at the time of faulting. *Central Research Institute of Electric Power Industry Report*, U87039, 18pp (in Japanese with English abstract).
[4] Hataya, R., Tanaka, K., 1993. Studies on applicability of fault dating by ESR method (1) -Experiments on zero-setting of ESR signals in quartz-. *Central Research Institute of Electric Power Industry Report*, U93019, 26pp (in Japanese with English abstract).
[5] Smith, E.H., Arnell, R.D., 2013. A new approach to the calculation of flash temperatures in dry, sliding contacts. *Tribology Letters*, 52, 407–414.

P-32

Spaciotemporal change of source parameters of repeaters due to the 2011 Tohoku-Oki earthquake

KAZUYA TATEIWA[1], TOMOMI OKADA[1], NAOKI UCHIDA[1], TOSHIO KONO[1]

[1] Department of Geophysics, Graduate School of Science, Tohoku University

A number of small to moderate repeating earthquakes occur at the upper boundary of subducting Pacific plate in NE Japan. Understanding the source characteristics of repeating earthquakes and their spaciotemporal changes gives us insight about the loading rate and its variation due to the plate motion and physical mechanisms of earthquakes, which can be common with major earthquakes because they would have the same occurrence structure as the small repeaters. In this study, we investigated the spatiotemporal change of source parameters of repeating earthquakes occurred on the Pacific interplate before and after the 2011 Tohoku-oki earthquake. We analyzed seismic waveforms from about 3,000 repeating earthquake groups and about 7,000 repeating earthquakes in total. In this study, we show the results obtained by analysis of repeaters located off-Kamaishi and near Iwaizumi, Iwate, NE Japan.

In off-Kamaishi, repeaters are observed in a very constant recurrence cycle (~5.5 yr) and magnitude (~4.9) before the Tohoku-oki earthquake, however, the recurrence interval was extremely shortened and the size of the earthquake was substantially enlarged immediately after the Tohoku-oki earthquake. The recurrence interval and magnitude are becoming close to those of before the Tohoku-oki earthquake with time. Although stress drop calculated with spectral ratio method is about 14 MPa before the Tohoku-oki earthquake, it is estimated that stress drop after the Tohoku-oki earthquake became smaller than before to have roughly a constant value (~2 MPa). The radius of ruptured fault estimated from corner frequency become about 5 times larger just after the Tohoku-oki earthquake and later it became about 1 km. The radius of rupture fault of post-Tohoku events is becoming close to that of pre-Tohoku event with time. These results agree with Uchida et al. (2015) [1] that estimated the rupture area of off-Kamaishi sequence by slip inversion. We consider that these changes of source parameters before and after the Tohoku-oki earthquake are caused by its afterslip.

On the other hand, the repeating earthquake sequences in Iwaizumi does not have obvious changes in magnitude and stress drop before and after the Tohoku-oki earthquake. If this region was less affected by afterslip than off-Kamaishi, small aftership might make the difference from the results of off-Kamaishi. We found the directivity estimated from corner frequency is observed only for repeaters of $M<4$, which indicates these small repeating earthquakes are composed of complex rupture. As it was suggested that repeaters of Iwaizumi sometimes rupture multiple patches in previous study, such complexities in rupture and the interaction between small ruptures would affect the recurrence of repeaters.

References

[1] Uchida, N., K. Shimamura, T. Matsuzawa, and T. Okada (2015), Postseismic response of repeating earthquakes around the 2011 Tohoku-oki earthquake: Moment increases due to the fast loading rate, J. Geophys. Res. Solid Earth, 120, doi:10.1002/2013JB010933.

P-33

Mechanism and frequency change of pressure oscillation in the laboratory geyser system

NORIKO TESHIMA[1], ATSUSHI TORAMARU[2]

[1] Department of Geophysics, Graduate School of Science, Tohoku University
[2] Department of Earth and Planetary Sciences, Faculty of Science, Kyushu University

Geysers are hydrothermal activities seen in volcanic areas, which exhibit characteristic behaviors such as cyclicity, time-predictability, etc. Geysers are known to show seismic events before eruptions, which have similarities with volcanic seismicity [1], and they have simpler material properties and more accessibility for observation than volcanos. Thus, understanding seismic events of geysers may provide potential insights into volcanic tremors, which are important signals in forecasting forthcoming eruptions. In natural geysers, it is known that pressure pulses occurring inside geyser's conduit excite tremors [2], but the source and mechanism of them are still unclear. Even in geysers, not to mention volcanos, natural phenomena are complex and hard to understand because their interiors are hardly observed directly and because there are additional factors such as the influence of atmospheric conditions. Therefore, simplified laboratory experiments which allow us to directly observe phenomena occurring in the interior may be useful for understanding natural phenomena. In this study, we tried to reveal the mechanism of pressure oscillation and factors controlling its dominant frequency using our fluid oscillation model and pressure and temperature data measured in our laboratory experiments.

We designed an experimental setup which reproduces cyclic eruptions of natural geysers. The setup mainly consisted of a flask and a glass tube, which correspond to natural hot water chamber and conduit, respectively. Heating the flask by the hotplate, we measured pressure and temperature in the flask, and erupted mass of each eruption. We also took video images of flask interior and water surface in the conduit with normal-speed and high-speed video cameras. From the movies of the water surface, we digitalized the vertical water column movement in the conduit using a video analysis software. We examined the effects of experimental conditions on characteristics of pressure oscillation by varying three geometric parameters of the experimental system: (i) inner flask volume, (ii) initial water level in the conduit, and (iii) cross-sectional area of the conduit. In interpreting experimental results, we used a model proposed by Toramaru et al. (Volcanological Society of Japan 2010 Fall Meeting). In this model, the frequency of pressure oscillation is represented in terms of geometric parameters of the experimental system and the effective bulk modulus K* of fluid in the flask. Using this model, we calculated theoretical values of the resonance frequency and compared it with the measured values of dominant frequency of pressure oscillation.

The results showed that the measured pressure oscillation in the flask consisted of high-frequency pulses and subsequent low-frequency damped oscillation, which were caused by the bubble formations in the flask and by the vertical water column movement in the conduit, respectively. From an eruption to the next eruption, the dominant frequency of pressure oscillation decreased systematically, which was explained by the reduction of K* as a result of increase in the gas volume fraction in the flask by heating. The variations in temporal behavior of dominant frequency could be interpreted by differences in the setting of geometric parameters and in the initial values of K* just after eruptions due to various erupted masses of the preceding eruptions.

In conclusion, the pressure oscillation in the experimental geyser system is caused by bubble formations in the flask and vertical water column movement in the conduit. The dominant frequency of pressure oscillation is controlled by the geometric parameters of the experimental system and the erupted mass of the preceding eruption.

References

[1] Kieffer, S.W., 1984. Seismicity of Old Faithful Geyser: an isolated source of geothermal noise and possible analogue of volcanic tremor. Journal of Volcanology and Geothermal Research 22, 59-96.
[2] Kedar, S., Kanamori, H., Sturtevant, B., 1996. The origin of harmonic tremor at Old Faithful Geyser. Nature 379, 708-711.

P-34

Evolutions of water mass anomalies in the upper North Pacific based on Argo data, in STMW, ESTMW, and CMW

TONG WANG[1], TOSHIO SUGA[1,2], SHINYA KOUKETSU[2]

[1] Department of Geophysics, Graduate School of Science, Tohoku University
[2] Research and Development Center for Global Change, Japan Agency for Marine-Earth Science and Technology

Under the background of climate changes, long-term trends and interannual to decadal variations of water masses have been discovered in recent studies. However, how they evolved in space and time is still not fully investigated, partly due to the insufficiency of observation. With spatially and temporally unbiased data available through Argo floats recently, this study describes three-dimensional evolutions of water mass anomalies during 2004-2015, focusing on three typical water masses in the upper North Pacific: North Pacific Subtropical Mode Water (STMW), Eastern Subtropical Mode Water (ESTMW), and North Pacific Central Mode Water (CMW).

In order to preserve the water mass characteristics as much as possible, the analysis in this study is mainly on neutral density surfaces, along which the advection and mixing of water masses dominantly occur. Because of the compensation between temperature and salinity on isopycnal surfaces, this study mainly investigates salinity as a proxy of spiciness. The preliminary findings are listed as follows:

In STMW:
The temporal variations of spiciness are dominated by interannual or longer variations. There is a long-term freshening trend at 0.005/year generally as well as strong decadal variations. The former is related to global warming; the latter are caused by the decadal variations of Kuroshio Extension path stability. These anomalies show rapid southwestward propagations in STMW, and the directions can be explained by geostrophic currents, but the propagation speed are 2-3 times higher than geostrophic currents, which indicates other processes involved. The origins of anomalies are most likely to be the STMW formation region. Another possible origin is found in the subtropics of the central North Pacific through statistical analysis, which needs further verification and explanation. Strikingly, the Eulerian temporal changes of spiciness are preserved well during the large distance propagation, implying the existence and persistence of large-scale spiciness fronts.

In ESTMW:
The temporal variability of ESTMW is higher than STMW and CMW, and interannual or longer variations are dominant. The long-term trend in northeastern ESTMW shows freshening, while the southwestern ESTMW is in salinification. There is an obvious 5-6-year oscillation cycle. The anomalies shift between positive and negative rapidly at the ESTMW formation region, spread to the whole ESTMW along its subduction path in each period, and propagate southwestward to the central subtropics and the western tropics by geostrophic flow.

In CMW:
Both spiciness and its total variations are smaller than the other two water masses, but the seasonal variations are higher, being comparable with interannual or longer variations in the northern CMW. With regard to trends, the northern CMW is in salinification, with the anomalies propagating eastward on both monthly scale and annual mean. However, the majority of CMW shows freshening almost uniformly, with weak but recognizable southward propagations.

In conclusion, this study provides a comprehensive description of the evolutions of water mass anomalies in the upper North Pacific for the first time. The regional variations that have been found by limited observations are confirmed and complemented with three-dimensional presentations. The evolutions occurred in earlier years and documented by previous studies are updated by the present analysis. Furthermore, the new phenomena that should be investigated in future are also raised.

P-35

Seasonal and latitudinal variations of the dayside N_2/CO_2 at 140 km altitude on Mars derived from MAVEN/IUVS

NAO YOSHIDA[1], HIROMU NAKAGAWA[1], NAOKI TERADA[1], HITOSHI FUJIWARA[2], IMAMURA TAKESHI[3], MAVEN/IUVS TEAM

[1] Graduate School of Science, Tohoku University
[2] Faculty of Science and Technology, Seikei University
[3] Department of Complexity Science and Engineering, Graduate School of Frontier Sciences, The University of Tokyo, Chiba, Japan

It is believed that liquid water was abundant on early Mars, despite Mars being too cold today to sustain significant amounts of liquid water. The most likely explanation is that early Mars had a more-effective greenhouse atmosphere and most part of atmosphere and water have lost to space. Mars Atmosphere and Volatile EvolutioN (MAVEN) mission was designed to explore the loss of gas to space at the present. MAVEN spacecraft revealed highly variable nature of the upper atmosphere in density, temperature, and atmospheric composition (e.g. Mahaffy et al., 2015; Elrod et al., 2017; Stone et al., 2018; Slipski et al., 2018). However, the controlling factor of the variations has yet to be fully characterized due to the limited spatial- and temporal- observing geometry by in-situ measurements. In addition to the effects by the external force, such as the solar wind and solar EUV on the upper atmosphere, the effect of lower atmospheric phenomena is also required to account for the substantial variations of the upper atmosphere. For instance, the homopause altitude (~120 km altitude) influences the upper thermospheric composition, thereby the species escaping to space [Imamura et al., 2016]. The fractionation between the homopause and the exobase determines the relative abundance of species to escape to space [Jakosky et al., 2017]. For this purpose, further investigation around the atmospheric boundary from the middle atmosphere to lower thermosphere is crucial for understanding regional coupling between the lower and upper atmosphere.

We have investigated the seasonal variation of the N_2/CO_2 ratio at 140 km altitude derived from ultraviolet spectroscopy remote-sensing measurements by Imaging Ultraviolet Spectrograph (IUVS) aboard MAVEN. We used the dataset of level 2 version 13 revision 1 data provided by the Planetary Data System, which includes retrieved CO_2 and N_2 number density profiles derived from dayglow emissions. We analyzed N_2 and CO_2 number densities observed from October 2014 to May 2018. Observations cover in the dayside from 7 to 19 hr. The observations covered almost all solar longitudes within the two Martian Years. The retrieved CO_2 density has small uncertainty but the retrieved N_2 density has relatively larger uncertainty in particular above ~170 km due to the dimmer emission intensity. For precise analysis of the N_2/CO_2 ratio, we confine our analysis to the data at 140 km altitude where N_2/CO_2 has uncertainty less than 50%. We found that the N_2/CO_2 ratio at 140 km altitude significantly varies in the range of 0.02 to 0.20, which shows an annual sinusoidal trend. The higher ratio appears during aphelion and the lower ratio appears during perihelion. CO_2 and N_2 number densities also have similar annual variations. It is noted that the CO_2 density varies by a factor of 100, while N_2 density by a factor of 10. This large CO_2 variation affects the N_2/CO_2 ratio at 140 km. The potential sources of the seasonal variation we found are variations (1) of the surface mixing ratio, (2) of the homopause altitude, and (3) of the thermospheric temperature. In this paper, the effect of surface mixing ratio is discussed using Mars Climate Database version 5.3 [Forget et al., 1999; Lewis et al., 1999]. We also address the effects of other sources by considering the seasonal variation of homopause altitude [Slipski et al., 2018] and background temperature [Bougher et al., 2017; Stone et al., 2018].

P-36

The composition of the Mars

TAKASHI YOSHIZAKI[1], WILLIAM F. MCDONOUGH[1,2,3]

[1] Department of Earth Science, Graduate School of Science, Tohoku University. (E-mail: takashiy@tohoku.ac.jp)
[2] Department of Geology, University of Maryland, College Park.
[3] Research Center of Neutrino Sciences, Tohoku University.

Compositional models of the terrestrial planets provide constraints on accretionary evolution of the inner solar system, styles and products of core-mantle and mantle-crust differentiation, and surface evolutionary processes. We present models of composition of Mars and its silicate and metallic fractions (bulk silicate Mars (BSM) and the core) that are based on chemical and isotopic abundances in Martian meteorites and satellite observations. The models are chemically and physically self-consistent, specifically matching planetary geodetic observations. Unlike previous models [1–3], we do not fix the planetary Mg/Si value as this ratio is variable in chondritic meteorites [4] and there are conflicting results for the solar ratio from different data sets. Refractory lithophile elements in the BSM are 2.4 times higher than that in CI carbonaceous chondrites (cf. 2.8×CI for the bulk silicate Earth [5]) and document a heterogeneous space/time distribution of refractory materials in the accretionary disk [6]. The lower Martian Mg/Si (0.88) as compared to the Earth's value (0.96 [5]) also reveals a time/space variation of Mg/Si (i.e., olivine to pyroxene ratio) during planetary accretion. The moderately volatile elements (MVE) are depleted in Mars, but less so than that for the Earth. The bulk chemical and isotopic composition of Mars is similar to H ordinary chondrites, albeit Mars being more depleted in MVE.

The Martian volatility trend restricts the core to having <5 wt% S [cf. 2, 3]. Light elements in the Martian core is a mixture of S, O and H in the proportions 3.6, 5.0, and 1.3 wt%, respectively. Thus, the Martian core's mass fraction is 23%, the core-mantle boundary is 1680 km deep, and there is no perovskititic lower mantle. A planetary Urey number of 0.86 is derived from an average surface heat flux of 19 mW/m^2 [7] and the BSM abundances of heat-producing elements. We advocate a smaller contribution from internal cooling during Mars thermal evolution [cf. 7, 8]. Core size and heat flux data from the InSight mission [9] will test our model for Mars.

References

[1] Morgan, J.W., Anders, E., 1979. Chemical composition of Mars. GCA 43, 1601–1610.
[2] Wänke, H., Dreibus, G., 1994. Chemistry and accretion history of Mars. Philos. Trans. Royal Soc. A 349, 285–293.
[3] Taylor, G.J., 2013. The bulk composition of Mars. Chem. Erde 73, 401–420.
[4] Wasson, J.T., Kallemeyn, G.W., 1988. Compositions of chondrites. Philos. Trans. Royal Soc. A 325, 535–544.
[5] McDonough, W.F., Sun, S.s., 1995. The composition of the Earth. Chem. Geol. 120, 223–253.
[6] Desch, S.J., et al., 2018. The effect of Jupiter's formation on the distribution of refractory elements and inclusions in meteorites. ApJS 238, 11.
[7] Parro, L.M., et al., 2017. Present-day heat flow model of Mars. Sci. Rep. 7, 45629.
[8] Plesa, A.C., et al., 2015. Thermal evolution and Urey ratio of Mars. JGR: Planets 120, 995–1010.
[9] Smrekar, S.E., et al., 2019. Pre-mission InSights on the interior of Mars. Space Sci. Rev. 213, 3.

P-37

Structure of H_2O-rich Mg_2SiO_4 melts at high pressure from *ab-initio* simulations

LIANG YUAN[1,2], GERD STEINLE-NEUMANN[2], AKIO SUZUKI[1], EIJI OHTANI[1]

[1] Department of Earth and Planetary Materials Science, Tohoku University, 980-8578 Sendai, Japan
[2] Bayerisches Geoinstitut, Universität Bayreuth, 95440 Bayreuth, Germany

Water is thought to play an essential role in Earth's dynamics, as it fundamentally alters the physical properties of mantle materials. An improved characterization of the incorporation mechanism of hydrogen in silicate magmas is crucial for our understanding of their structure–property relations, i.e., to determine the chemical and physical processes of magma formation and evolution. Contrary to the small overall budget of H_2O in the mantle, melting experiments suggest that hydrous melts in equilibrium with depleted peridotites are extremely water-rich (~26 wt% H_2O) and ultramafic in composition at typical mantle temperatures [1,2]. Similarly, *in situ* observations on partial melting of hydrous peridotites also show a large amount of water, up to 16.5 wt% H_2O, can be dissolved in partial ultramafic melts at the base of the upper mantle [3]. These melts are far too water-rich to be neutrally buoyant, although it is generally accepted that iron tends to be enriched in melts [4], which may increase their density substantially. A broad range of water content needs to be considered for properties of hydrous silicate melts, beyond prior experiments and simulations. Here we conduct first-principles molecular dynamics simulations on water-rich Mg_2SiO_4 melts (with up to 16.5 wt% H_2O) at 0–15 GPa and 1800–2200 K relevant to upper mantle conditions, with the goal of understanding the structure and thermodynamic properties of H_2O-bearing silicate melts. We evaluate the simulation results in terms of the structure of the hydrous melts, i.e., radial distribution functions (RDFs), coordination and speciation. In some simulations we find support of experimental data [5,6] that observe an anomalous pressure dependence in the location of the first sharp diffraction peak (FSDP) in the liquid structure factors $S(q)$ from the weighted Fourier transform of the RDFs, and the occurrence of a satellite peak at q position just above the FSDPs. This unusual behavior has been interpreted before as lengthening of the silicate network ordering [5,6]. In our simulations, however, we find from an analysis of the partial RDFs that this is caused by the increase in the pair interaction between Si and Si, and decrease in the pair interaction between Si and H.

References

[1] Novella, D. *et al.* Melting phase relations in the systems Mg_2SiO_4–H_2O and $MgSiO_3$–H_2O and the formation of hydrous melts in the upper mantle. *Geochim. Cosmochim. Acta* **204**, 68–82 (2017).
[2] Myhill, R., Frost, D. J. & Novella, D. Hydrous melting and partitioning in and above the mantle transition zone: Insights from water-rich MgO–SiO_2–H_2O experiments. *Geochim. Cosmochim. Acta* **200**, 408–421 (2017).
[3] Freitas, D. *et al.* Experimental evidence supporting a global melt layer at the base of the Earth's upper mantle. *Nat. Commun.* **8**, 2186 (2017).
[4] Nomura, R. *et al.* Spin crossover and iron-rich silicate melt in the Earth's deep mantle. *Nature* **473**, 199–202 (2011).
[5] Yamada, A. *et al.* In situ X-ray experiment on the structure of hydrous Mg-silicate melt under high pressure and high temperature. *Geophys. Res. Lett.* **34**, L10303 (2007).
[6] Yamada, A. *et al.* In situ X-ray diffraction study on pressure-induced structural changes in hydrous forsterite and enstatite melts. *Earth Planet. Sci. Lett.* **308**, 115–123 (2011).

P-38

An experimental approach to a multiple saturation point of the "direct ascent" petit-spot basalts

TAKU YUTANI[1,2], PIERRE CONDAMINE[2,3], NAOTO HIRANO[1], CATHERINE MCCAMMON[2], DANIEL FROST[2]

[1] Tohoku University
[2] University of Bayreuth
[3] University of Lorraine

Asthenosphere as the seismic low-velocity zone at the upper mantle of the earth plays an important role in stabilizing plate tectonics. Although the geochemical and petrological properties of the asthenosphere are essential to understand the surface environment of terrestrial planets, nature of the asthenosphere is still enigmatic. Petit-spot is a new-type monogenic volcano discovered at the beginning of the 21st century. Because of the age and eruption setting of the petit-spot sea knolls (the eruption age is much younger than surrounding crustal rocks), it is proposed that petit-spot magma has been generated inside the asthenospheric mantle and it can have crucial information on the asthenosphere. Petrographical and geochemical data of the petit-spot alkaline basalts, however, suggest that previously reported petit-spot samples from the Northwest Pacific Ocean have undergone some degrees of fractional crystallization of olivine and/or clinopyroxene etc. and have assimilated with ambient lithospheric mantle. Thus, their chemical composition might have been considerably modified before the eruption. On the other hand, the samples newly collected from three isolated knolls show strongly primitive geochemical characteristics such as low-silica, high alkali and high volatile element contents. The rapid ascending ratios are estimated for three primitive lavas by Fe-Mg diffusion of olivine xenocrysts, so-called "direct ascent" melts.

Although the "direct ascent" petit-spot magmas do not seem to have undergone assimilation with surrounding mantle peridotite while ascending, the samples of the volcanic rocks contain quite a few amount of olivine phenocrysts and have relatively high vesicularity (around 15 vol. %), which means these magmas have undergone certain amount of olivine-fractional crystallization and degassing of volatile elements such as H_2O and/or CO_2.

We calculated H_2O and CO_2 contents of three "direct ascent" petit-spot samples from the NW Pacific plate before the degassing with presuming closed system and equilibrium degassing from their vesicularities and H_2O and CO_2 contents in the glass. The calculated volatile contents of H_2O and CO_2 are 2.0-2.4 wt% and 1.0-5.0 wt%, respectively. Chemical compositions of olivines equilibrated with the melt are calculated from partition coefficients of Mg, Fe, Mn and Ni between olivine and melt. According to our calculation, the "direct ascent" petit-spot melt were equilibrated with the mantle peridotite before ~25 mol% of the olivine fractionation.

Now, we have primary compositions of the "direct ascent" petit-spot magmas. Multiple saturation points of the "direct ascent" petit-spot lavas will be a powerful tool to elucidate the geochemical and petrological properties of the asthenosphere because they reveal P-T conditions and lithologies where primary melt lastly equilibrated with. For this, we are investigating multiple saturation points by piston cylinder experiments. Although we have not found the saturation points at the moment, we have found phlogopite which is equilibrated with one of the primary melts at 1,300 ºC and 2.8 GPa. That implies the liquidus phase of the primary melt is possibly phlogopite peridotite, to put it another way, so-called recycled mantle has likely produced the "direct ascent" petit-spot magmas in the asthenosphere.

This project is supported by the JSPS Japanese-German Graduate Externship.

Presenter list

	Name (First, Middle, Last)	Affiliation	E-mail address
1	Geri Agroli	Dept. of Environmental Studies for Advanced Society, Tohoku Univ.	geri@geo.kankyo.tohoku.ac.jp
2	Kana Amano	Dept. of Earth Science, Tohoku Univ.	amakana@dc.tohoku.ac.jp
3	Frederick M. Bingham	Dept. of Physics and Physical Oceanography, Univ. of North Carolina Wilmington	binghamf@uncw.edu
4	Serena Dominijanni	Bayerisches Geoinstitut, Univ. of Bayreuth	Serena.Dominijanni@uni-bayreuth.de
5	Lisa Eberhard	Bayerisches Geoinstitut, Univ. of Bayreuth	Lisa1.Eberhard@uni-bayreuth.de
6	Sara Emanuel	Dept. of Earth Science, Tohoku Univ.	saraemanuel17@gmail.com
7	Wakana Fujita	Dept. of Earth Science, Tohoku Univ.	w.fujita@dc.tohoku.ac.jp
8	Julien Gasc	Laboratoire de Géologie, Ecole Normale Supérieure de Paris	gasc@geologie.ens.fr
9	Asteria S. Handayani	Dept. of Earth Science, Tohoku Univ.	asteria.satyaning.handayani.s2@dc.tohoku.ac.jp
10	Mohammad Hasib	Dept. of Geophysics, Tohoku Univ.	hasib@dc.tohoku.ac.jp
11	Takashi Hirose	Dept. of Geophysics, Tohoku Univ.	takashi.hirose.r6@dc.tohoku.ac.jp
12	Yongsheng Huang	Dept. of Earth Science, Tohoku Univ.	huang.yongsheng.s8@dc.tohoku.ac.jp
13	Mizuki Iida	Dept. of Geophysics, Tohoku Univ.	mizuki.iida.r1@dc.tohoku.ac.jp
14	Takuma Ikegaya	Research Center for Prediction of Earthquakes and Volcanic Eruptions, Dept. of Geophysics, Tohoku Univ.	takuma.ikegaya.s1@dc.tohoku.ac.jp
15	Yoichi Inai	Center for Atmospheric and Oceanic Studies, Dept. of Geophysics, Tohoku Univ.	yoichi_inai@tohoku.ac.jp
16	Ayumu Ishikawa	Dept. of Geophysics, Tohoku Univ.	ayumu.ishikawa.t2@dc.tohoku.ac.jp
17	Mochamad R. Iskandar	Dept. of Geophysics, Tohoku Univ.	mriza@dc.tohoku.ac.jp
18	Mayu Kakefuda	Dept. of Earth Science, Tohoku Univ.	mayu.kakefuda.r4@dc.tohoku.ac.jp
19	Kazuki Machida	Dept. of Earth Science, Tohoku Univ.	kazuki.machida.p5@dc.tohoku.ac.jp
20	Enrico Marzotto	Bayerisches Geoinstitut, Univ. of Bayreuth	Enrico.Marzotto@uni-bayreuth.de
21	Caterina Melai	Bayerisches Geoinstitut, Univ. of Bayreuth	Caterina.Melai@uni-bayreuth.de
22	James D. P. Moore	Earth Observatory of Singapore, Nanyang Technological Univ.	james.moore@ntu.edu.sg
23	Mayumi Mujin	Dept. of Earth Science, Tohoku Univ.	mayumi.mujin.a5@tohoku.ac.jp
24	Jun Muto	Dept. of Earth Science, Tohoku Univ.	jun.muto.a3@tohoku.ac.jp
25	Yuki Nakamura	Dept. of Geophysics, Tohoku Univ.	y.nakamura@pat.gp.tohoku.ac.jp

	Name (First, Middle, Last)	Affiliation	E-mail address
26	Theodorus Permana	Dept. of Geophysics, Tohoku Univ.	theodorusp@dc.tohoku.ac.jp
27	Marija Putak Juricek	Bayerisches Geoinstitut, Univ. of Bayreuth	Marija.Putak-Juricek@uni-bayreuth.de
28	Kelvin Richards	International Pacific Research Center, Sch. of Ocean and Earth Science and Technology, Univ. of Hawai‘i at Mānoa	rkelvin@hawaii.edu
29	Greta Rustioni	Bayerisches Geoinstitut, Univ. of Bayreuth	Greta.Rustioni@uni-bayreuth.de
30	Niccolò Satta	Bayerisches Geoinstitut, Univ. of Bayreuth	Niccolo.Satta@uni-bayreuth.de
31	Martha Savage	Sch. of Geography, Environment and Earth Sciences, Victoria Univ. of Wellington	martha.savage@vuw.ac.nz
32	Sando Sawa	Dept. of Earth Science, Tohoku Univ.	sando.sawa.t1@dc.tohoku.ac.jp
33	Ross S. Stein	Temblor, Inc. / U.S. Geological Survey	ross@temblor.net
34	Gerd Steinle-Neumann	Bayerisches Geoinstitut, Univ. of Bayreuth	g.steinle-neumann@uni-bayreuth.de
35	Shunsuke Sugimura	Dept. of Geophysics, Tohoku Univ.	shunsuke.sugimura.t4@dc.tohoku.ac.jp
36	Manami Suzuki	Research Center for Prediction of Earthquakes and Volcanic Eruptions, Dept. of Geophysics, Tohoku Univ.	manami.suzuki.p8@dc.tohoku.ac.jp
37	Benoit Taisne	Earth Observatory of Singapore, Nanyang Technological Univ.	BTaisne@ntu.edu.sg
38	Miki Takahashi	Dept. of Earth Science, Tohoku Univ.	miki.takahashi.p4@dc.tohoku.ac.jp
39	Naoko Takahashi	Dept. of Earth Science, Tohoku Univ.	naoko.takahashi.t1@dc.tohoku.ac.jp
40	Naoya Takahashi	Center for Atmospheric and Oceanic Studies, Dept. of Geophysics, Tohoku Univ.	naoya.takahashi.r5@dc.tohoku.ac.jp
41	Naoya Takahashi	Dept. of Earth Science, Tohoku Univ.	naoya.takahashi.t1@dc.tohoku.ac.jp
42	Hideko Takayanagi	Dept. of Earth Science, Tohoku Univ.	hideko.takayanagi.b4@tohoku.ac.jp
43	Kiriha Tanaka	Dept. of Earth Science, Tohoku Univ.	kiriha.tanaka.s8@dc.tohoku.ac.jp
44	Kazuya Tateiwa	Research Center for Prediction of Earthquakes and Volcanic Eruptions, Dept. of Geophysics, Tohoku Univ.	kazuya.tateiwa.r7@dc.tohoku.ac.jp
45	Noriko Teshima	Dept. of Geophysics, Tohoku Univ.	noriko.teshima0430@gmail.com
46	Tong Wang	Dept. of Geophysics, Tohoku Univ.	wangtong.330@gmail.com
47	Nao Yoshida	Dept. of Geophysics, Tohoku Univ.	n.yoshida@pat.gp.tohoku.ac.jp
48	Takashi Yoshizaki	Dept. of Earth Science, Tohoku Univ.	takashiy@tohoku.ac.jp
49	Liang Yuan	Dept. of Earth Science, Tohoku Univ.	yuan.liang.s4@dc.tohoku.ac.jp
50	Taku Yutani	Dept. of Earth Science, Tohoku Univ.	t.yutani@dc.tohoku.ac.jp